Politecnico di Torino

Master's Degree in Aerospace Engineering

Graduation Session July 2026

Hybrid Trajectory Optimization for Missions from Lagrangian Points in the Earth-Moon System

Tutors:
Lorenzo Casalino

Candidate:
Ferdinando Grimaldi

A mamma e papà,
a loro devo tutto.

Abstract

This Master's thesis aims to compute optimised orbital transfers in the Earth-Moon system using a hybrid optimisation framework combining a Genetic Algorithm, for global solution search, and Sequential Quadratic Programming, for local refinement. The following topics are analysed at a theoretical level: the main operational and future missions in the cislunar environment, in order to provide a broad overview of the explored space scenario; the fundamental astrodynamics needed to understand the physical mechanisms of the problem; and the state of the art of the optimisation algorithms used to fully exploit their capabilities. The optimised trajectories are referenced to the NRHO of a similar-Lunar Gateway mission and to circular orbits around the Earth and the Moon. Several trajectories are tested in order to predict the behaviour of fuel consumption as a function of various parameters, such as the number of impulses, the inclination of the target orbit, and the total flight time of the transfer. The results obtained demonstrate the effectiveness of the hybrid approach used for the optimisations, with significant advantages in the reduction of the total ΔV of the transfers and in the reduced computational times achieved. The comparison among the derived trajectories reveals patterns that are useful for selecting the optimal transfer under fixed boundary conditions, such as final inclination or time of flight. The developed algorithm is also well-suited to more complex optimisation scenarios and provides fast and reliable solutions to the class of astrodynamic problems examined.

Table of Contents

List of Tables

List of Figures

Glossary

CAPSTONE

Cislunar Autonomous Positioning System Technology Operations and Navigation Experiment: A technology demonstrator and pathfinder mission for the Lunar Gateway. (Pages: 2, 5, 6, 9)

CR3BP

Circular Restricted Three-Body Problem: Astrodynamic model used to study the motion of a spacecraft under the gravitational influence of two primary bodies moving in circular orbits. (Pages: 2, 14, 15, 17, 18, 24)

CSA

Canadian Space Agency: International partner in the Lunar Gateway program. (Page: 8)

ECLSS

Environmental Control and Life Support System: System providing life support for the crew, source of non-gravitational perturbations on the spacecraft. (Page: 7)

ECI

Earth-Centered Inertial: Geocentric inertial reference frame used for trajectory propagation. (Page: 37)

EPRM

Extended Perilune Rendezvous Method: A bi-elliptical or low-energy trajectory method for lunar transfers. (Pages: 57, 66)

ESA

European Space Agency: International partner in the Artemis and Gateway programs. (Pages: 3, 8)

FPS

Fitness Proportionate Selection: A selection strategy used in Genetic Algorithms to form the mating pool. (Page: 28)

GA

Genetic Algorithm: A stochastic global search optimization algorithm inspired by biological evolution. (Pages: 1, 2, 26, 27, 28, 30, 31, 33, 34, 40, 44, 55, 60, 64, 65, 66, 67)

HLS

Human Landing System: Vehicle planned for lunar surface descent and ascent in the Artemis program. (Page: 53)

ISS

International Space Station: Low Earth orbit modular space station. (Page: 8)

JAXA

Japan Aerospace Exploration Agency: International partner in the Lunar Gateway program. (Pages: 8, 57)

JPL

Jet Propulsion Laboratory: NASA research and development center, developer of the SPICE toolkit. (Pages: 14, 23, 36)

LEO

Low Earth Orbit: Earth-centered orbit close to the planet's surface. (Pages: 1, 8, 10, 13, 40, 41, 42, 43, 46, 50, 66)

LLO

Low Lunar Orbit: Moon-centered orbit close to the lunar surface. (Pages: 1, 40, 52, 53, 55, 57, 66)

LPO

Libration Point Orbit: Trajectories oscillating around the Lagrangian equilibrium points. (Pages: 18, 19)

MBRSC

Mohammed bin Rashid Space Centre: International partner in the Lunar Gateway program. (Page: 8)

NASA

National Aeronautics and Space Administration: United States federal government space agency leading the Artemis program. (Pages: 1, 3, 5, 6, 7, 8, 9, 22, 23, 32, 36, 37, 42, 67)

NLP

Nonlinear Programming: Mathematical formulation for finite-dimensional optimization problems. (Pages: 26, 32)

NRHO

Near Rectilinear Halo Orbit: Highly elliptical, stable periodic orbit selected for the Lunar Gateway. (Pages: 1, 5, 8, 9, 13, 21, 22, 23, 24, 39, 41, 43, 47, 52, 53, 55, 57, 59, 62, 66, 67)

OCP

Optimal Control Problem: Mathematical formulation for determining a control policy that minimizes a cost function over time. (Pages: 25, 32)

OTC

Outbound Trajectory Correction: Correction maneuvers performed during the outbound leg of a lunar mission. (Pages: 7, 8)

RTC

Return Trajectory Correction: Correction maneuvers performed during the return leg of a lunar mission. (Page: 8)

SPICE

Spacecraft Planet Instrument C-matrix Events: NASA/JPL toolkit and data system for ephemerides and space mission geometry. (Pages: 23, 36, 37)

SQP

Sequential Quadratic Programming: A deterministic local refinement optimization algorithm. (Pages: 1, 26, 31, 32, 33, 34, 40, 44, 45, 55, 60, 64, 65, 66)

TDB

Barycentric Dynamical Time: Time scale used for highly accurate astronomical and astrodynamic calculations. (Page: 37)

ToF

Time of Flight: The total duration of an orbital transfer. (Pages: 1, 39, 66, 67)

ΔV

Delta-V (Velocity Variation): Measure of the impulse required to perform a maneuver, directly related to propellant consumption. (Passim, see e.g., Pages: 1, 7, 13, 25, 26, 38, 40, 42, 43, 49, 53, 57, 65, 66)

Chapter 1

Introduction

Since the end of the Apollo era, the perspective on lunar exploration has profoundly shifted. The international space community, led by NASA's Artemis program and supported, is no longer aiming for brief, single-shot landings, but rather for a sustainable, long-term human presence in the cislunar environment. A key point of this new architecture is the Lunar Gateway, an orbital outpost that will serve as a staging node for both lunar surface descents and future deep-space missions to Mars. Although NASA has recently announced an indefinite pause on the Gateway's assembly to prioritize the development of a lunar surface base, the NRHO remains a fundamental astrodynamic hub. Studying optimized trajectories to these orbits continues to be of critical interest, as they provide an ideal, highly stable staging environment for any future commercial or robotic operations in cislunar space.

Unlike traditional low Earth orbit stations, the Gateway will reside in a Near Rectilinear Halo Orbit. Operating in this highly nonlinear, N-body dynamical environment presents unprecedented astrodynamic challenges. Trajectories within cislunar space are governed by the chaotic gravitational interactions of the Earth, Moon, and Sun, rendering classical Keplerian mechanics insufficient for mission planning. In this regime, even minor perturbations can lead to rapid trajectory divergence, requiring precise orbital control and optimal transfer strategies to minimize propellant consumption and extend mission lifetimes.

To navigate and exploit this complex dynamical landscape, advanced numerical optimization techniques are strictly required. The objective of this Master's thesis is to compute and analyze optimized orbital transfers in the Earth-Moon system, specifically focusing on maneuvers departing from the Gateway's NRHO towards Low Earth Orbit and Low Lunar Orbit. To overcome the intrinsic limitations of single optimization algorithms, such as the global blindness of deterministic methods and the local inaccuracy of stochastic ones, this work develops and implements a robust hybrid optimization framework. By combining a Genetic Algorithm for global solution search with Sequential Quadratic Programming for exact local refinement, the solver automatically identifies high-precision, minimum-ΔV trajectories.

The thesis is structured into several consecutive chapters. Chapter 2 provides an overview of modern lunar missions, detailing the scientific objectives, the Artemis program, the Lunar Gateway, and the CAPSTONE pathfinder mission, framing the operational context of the work. Following this, Chapter 3 delves into the theoretical astrodynamics, transitioning from the classical Two-Body Problem to the Circular Restricted Three-Body Problem, and finally defining the N-body ephemeris model and stable periodic orbits like the NRHOs. Chapter 4 reviews the state of the art in trajectory optimization, introducing the mathematical formulation of the Genetic Algorithm and the SQP algorithm, while explaining the rationale and logic behind their hybridization. The computational methodology is then detailed in Chapter 5, including the setup of the optimization inputs, the trajectory propagation utilizing the NASA SPICE toolkit, and the implementation of fitness functions and constraints. Chapter 6 presents the core results of the research, analyzing optimal maneuvers from NRHO to LEO and LLO, and evaluating the impact of the number of impulses, target inclinations, and time of flight on the overall propellant consumption. Finally, Chapter 7 summarizes the findings, highlighting the effectiveness of the hybrid solver and outlining the physical insights gained from the computed trajectories.

Chapter 2

Lunar Missions

2.1 Scientific objectives of lunar missions

Since the end of the Apollo program, which saw humanity's first steps on the lunar surface between the 1960s and 1970s, the prospect of a human return to the Moon has been the subject of continuous debate and feasibility studies, which however did not translate into actual flight missions for decades. The current exploration architecture, led by NASA through the Artemis program and supported by a solid network of international partners such as the ESA, brings an end to a deadlock lasting over forty years, proposing a concrete, pragmatic, and above all sustainable exploration campaign [1, 2, 3].

Unlike the typical approach of the past, the current return does not aim simply to replicate engineering milestones already achieved, but is designed from the outset to ensure long-term use of our satellite for scientific, exploratory, and economic benefit [4].

To ensure the feasibility of this new space era, agencies have adopted a rigorous systems engineering approach. Historically, missions were often developed using a capability-based approach, i.e., based on the development of specific technological capabilities or vehicles at a given time. The current cislunar strategy, instead, is based on an objective-based paradigm: before defining implementation details and launch architectures, the reasons and objectives of exploration are established upfront, structured into fundamental areas ranging from planetary science to the development of interoperable infrastructures. The primary intent is in fact to create a global lunar utilization infrastructure that enables a continuous presence, both human and robotic, fostering a robust economy in which governmental space agencies are not the only users [1].

From a scientific point of view, interest in the Moon is driven by an unprecedented discovery potential. Our satellite is considered a true time capsule dating back

4.5 billion years. Its geological record, not having been altered over time by tectonic processes or atmospheric erosion as on Earth, preserves intact traces of primordial planetary evolution and provides crucial clues about the evolution of the Earth–Moon system, the Sun, and the rocky planets [3, 4].

The lunar surface also offers exceptional opportunities for research in fields such as astronomy, astrobiology, fundamental physics, and human and biological sciences for understanding organism responses to the space environment. Although many scientific investigations can be conducted without human presence, the full achievement of these ambitious objectives necessarily requires the resumption of human operations on the surface [3]. The in-situ presence of human explorers, operating in synergy with surface and orbital robotic systems, represents the most effective method for addressing high-priority scientific questions. Supporting this architecture is a deeply renewed commercial and regulatory ecosystem [1]. Through initiatives such as the Commercial Lunar Payload Services program, the acquisition of lunar delivery services directly from private commercial providers has been promoted, fostering industrial growth and providing agility in testing technologies that will later be crucial for crewed missions [4].

On the geopolitical level, this complex network of operations is regulated by the Artemis Accords, established in 2020 and now signed by dozens of nations, which provide a set of common principles to ensure that the exploration and use of outer space proceed in a peaceful, responsible, and standardized manner. In this broad and renewed context, the Moon stops to be considered a mere end goal and becomes a vital strategic outpost [4].

The technologies required to survive and work independently from Earth will undergo their first testing in the lunar environment, before being extended toward more distant deep space destinations [5]. To support such extended exploration, the creation of supporting space stations designed to operate far from the strong gravitational influence of Earth and to facilitate descents to the lunar surface is essential. It is precisely in this scenario of cislunar settlement that the need arises to design innovative mission architectures and to study specific orbital trajectories capable of ensuring stability and continuous communications, with optimized energy expenditure for maintaining these new outposts [5].

2.2 Modern Lunar Programs

To turn into reality the strategic objectives of lunar exploration described above, the international space community has developed an unprecedented technological and operational infrastructure. The current architecture differs significantly from the single-shot missions of the past, relying instead on a complex network of launch vehicles, crew spacecraft, orbital stations, and commercial landing systems. This section analyzes in detail the three main pillars of the current cislunar exploration campaign: the transport architecture of the Artemis program, the development of the Lunar Gateway as an orbital hub, and the CAPSTONE pathfinder mission for validating orbital dynamics.

2.2.1 CAPSTONE mission

Given the innovative and previously untested nature of the selected NRHO orbit for the Gateway, NASA considered it necessary to first validate the dynamical environment through a cutting-edge exploratory mission. This role is fulfilled by CAPSTONE (Cislunar Autonomous Positioning System Technology Operations and Navigation Experiment), a technology demonstrator that serves as a pathfinder for the Lunar Gateway and the entire Artemis campaign.

Built in collaboration with commercial partners such as Advanced Space and Terran Orbital, CAPSTONE is a small CubeSat weighing only 25 kg. Launched on June 28, 2022, it underwent a four-month propulsion-assisted journey before successfully performing orbital insertion on November 13, 2022. From the standpoint of celestial mechanics, CAPSTONE became the first spacecraft ever to enter a southern NRHO around the Earth–Moon system's L2 Lagrange point. This trajectory is characterized by a 9:2 lunar synodic resonance and an orbital period of approximately 6.5 days.

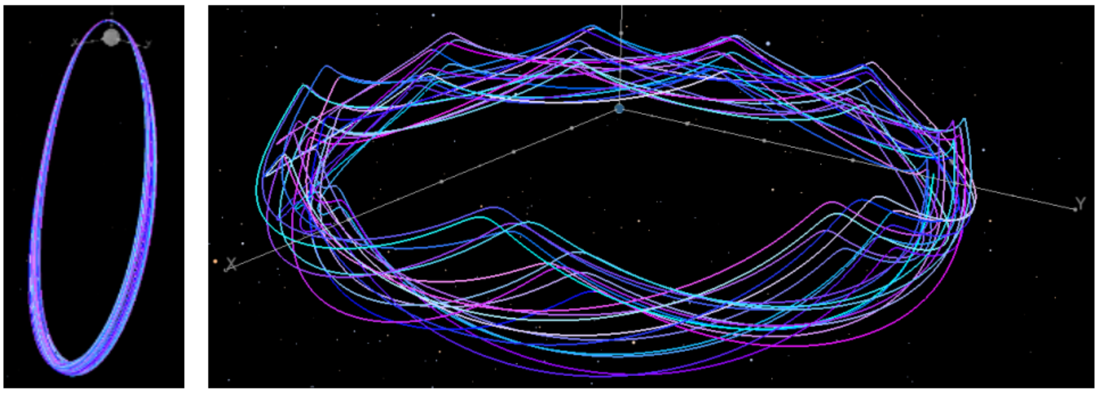

Figure 2.1: Trajectory of CAPSTONE [6].

During its primary mission and subsequent extension, the spacecraft achieved multiple key milestones for the engineering validation of the Gateway architecture, operating in a highly nonlinear dynamical environment.

The mission validated in-flight the mathematical models and propulsive requirements for station-keeping. The operational planning includes station-keeping maneuvers computed on 10-day tracking intervals and strategically placed each orbit between 180° and 200° of true anomaly relative to the Moon. Despite the mission having to manage a significant hardware anomaly, an engine locked in the open position that generates unpredictable disturbances on the vehicle, the post-flight data analysis demonstrated excellent results. The estimated navigation uncertainties remained consistently below the stringent requirements imposed by the Gateway program, below 10 km in position and 10 cm/s in velocity, for over 98% of the time spent in orbit.

CAPSTONE successfully tested the Cislunar Autonomous Positioning System, an innovative navigation software designed to compute the spacecraft's position fully autonomously. This peer-to-peer system communicates directly with NASA's Lunar Reconnaissance Orbiter, radiometrically measuring relative distance and its rate of change. This allows the spacecraft to update its state vector without relying exclusively on the costly tracking provided by the ground-based Deep Space Network antennas.

The technical impact of CAPSTONE on future orbital optimization studies is of inestimable value. The empirical data collected on real navigation performance, maneuver execution errors, and the influence of stochastic perturbations is refining ground-based estimation filters, drastically reducing uncertainties for Gateway operational planning. Precisely due to the importance of these as-flown data, the mission was extended until December 2025, serving as a continuous monitoring probe for the environment in which the assembly of the largest human outpost in deep space will soon begin [7, 6].

2.2.2 Artemis program

The Artemis program represents the execution framework through which NASA, in collaboration with international commercial partners, is conducting progressively complex human exploration missions, laying the foundations for a sustainable future presence on the Moon and for Mars exploration. The fundamental infrastructure for deep space access relies on two key elements: the super-heavy Space Launch System and the Orion spacecraft. The launch vector is currently the only vehicle capable of sending Orion, crew, and payloads directly to the Moon in a single launch, providing an unprecedented mass, volume, and initial energy capability. The system is supported on the ground by the Exploration Ground Systems infrastructure at Kennedy Space Center, responsible for assembly and launch operations.

The Artemis program is structured according to a mission manifest in which engineering complexity progressively increases. After the success of the uncrewed inaugural mission Artemis I in 2022, which validated Orion's heat shield and basic systems on a cislunar trajectory, the program will begin using commercial landers starting from Artemis III, scheduled for 2027, for the first lunar landings. From Artemis IV and V onward, starting in 2028, the architecture will use the upgraded of the launch system configuration for co-manifested missions aimed at assembling the Lunar Gateway in NRHO and deploying advanced surface infrastructure [4].

However, the key step for the transition toward these complex orbital operations is represented by Artemis II, the first mission to bring a human crew back into the lunar environment in over fifty years.

Unlike the subsequent landing missions, the Orion spacecraft on Artemis II will follow a free-return trajectory, conceptually similar to that used during the historic Apollo 8. The mission, lasting approximately 8 days, includes a lunar flyby of the far side of the Moon before being re-inserted, thanks to the Moon's gravitational influence, into a safe return path toward Earth.

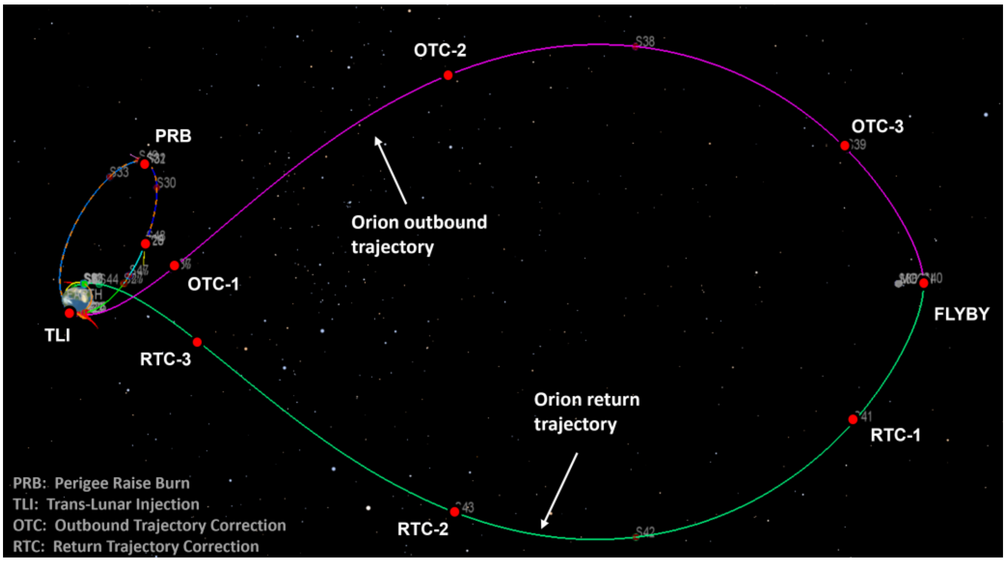

Figure 2.2: Notional Orion Free-Return Trajectory for the NASA Artemis II Mission [8].

From a theoretical point of view, a free-return trajectory is designed such that no additional translational maneuver is required after the burn that injects the spacecraft into the lunar transfer trajectory. In real operations, however, maintaining such a sensitive orbit requires periodic correction maneuvers due to numerous stochastic and dynamic uncertainties. Among the main disturbing factors are maneuver execution errors, navigation system uncertainties, and a set of non-gravitational perturbations generated by the crew's presence itself. Orion, for instance, experiences disturbances arising from the ECLSS, including outgassing, wastewater venting, the ammonia sublimator, as well as attitude adjustments and solar radiation pressure.

To ensure crew safety, the mission architecture includes a series of Outbound Trajectory Correction (OTC) maneuvers during the outbound leg and Return

Trajectory Correction (RTC) maneuvers during the return leg. The placement of these burns is a classical orbital optimization problem, governed by extremely strict constraints; for example, the closest approach point must never drop below 100 km from the lunar surface, and the total ΔV budget for correction maneuvers is limited to a maximum of 20 m/s.

Orion re-enters Earth's atmosphere following a strict flight corridor. The entry interface parameters, including down-range position, flight path angle, velocity magnitude, and cross-track position, must be maintained within tight tolerances to avoid atmospheric skip-out or fatal deceleration.

Arbitrary placement of OTC and RTC maneuvers would lead to excessive propellant consumption and likely violation of Entry Interface requirements. To address this challenge, the Artemis II planning used robust trajectory optimization techniques. These architectures employ linear covariance analysis models integrated into genetic algorithms to evaluate vehicle response by jointly considering the primary navigation system, based on the Deep Space Network and onboard sensors, and the backup system based on autonomous optical navigation [8].

The optimization of ΔV tested on Artemis II represents the fundamental mathematical and engineering basis required to address the subsequent, far more complex station-keeping and rendezvous operations required by NRHO orbits that will be used for maintaining the Lunar Gateway.

2.2.3 Lunar Gateway

A fundamentally disruptive element compared to past exploration paradigms is the realization of the Lunar Gateway, the first international space station designed to orbit the Moon. Unlike the ISS, which operates in LEO, the Gateway represents a true deep-space outpost, designed to operate highly autonomously and host crews during Artemis missions.

The project is the result of a major global effort led by NASA, with essential contributions from the world's major space agencies such as ESA, CSA, JAXA, and MBRSC, which will provide habitation modules, propulsion systems, next-generation robotic arms and logistics modules. From a scientific and operational perspective, the station will serve as a privileged laboratory for studying the interplanetary environment, in particular for analyzing solar and cosmic radiation outside Earth's magnetosphere, and as a staging post for transfers to the lunar surface and, in the future, to Mars [9, 10].

However, the most innovative engineering feature of the Gateway lies in its trajectory: the station will reside in a polar NRHO characterized by a specific 9:2 lunar synodic resonance, i.e., 9 revolutions every two lunar months. This is a highly elliptical and unusual orbit, bringing the spacecraft as close as 1,500 km above the lunar north pole and then as far as nearly 70,000 km at apolune. This choice is not arbitrary and provides an ideal strategic compromise: proximity at perilune enables low-energy transfers to the lunar surface, while the large distance at apolune allows incoming spacecraft from Earth to intercept the station with great ease and propulsive efficiency [9].

However, long-term operation in such a dynamical environment governed by complex and chaotic N-body gravitational interactions of the Earth–Moon–Sun system is a challenge that justifies and makes necessary the use of advanced orbital optimization tools. To ensure a mission lifetime exceeding 15 years, mission planners must continuously solve intrinsically nonlinear optimization problems such as station-keeping. Due to external perturbations and natural orbital instabilities, the station requires periodic correction maneuvers. The objective of optimization tools is to compute trajectories that minimize fuel consumption while ensuring long-term vehicle stability.

Another issue is eclipse avoidance, due to strict thermal and power generation constraints, the Gateway cannot remain in Earth's or Moon's shadow for more than 90 minutes. Since the system geometry evolves over time, the station is periodically at risk of prolonged eclipses. Analysts must therefore design proactive orbital phase-change strategies.

Determining when, how, and with what magnitude to fire thrusters to modify the station's orbital phase while minimizing resource consumption is not a problem solvable with classical orbital mechanics. It is precisely in this operational need space that trajectory optimization algorithms come into play, such as those based on multiple-shooting techniques, which constitute the mathematical core and fundamental prerequisite for the safety and survival of future human infrastructures in the cislunar environment [11].

It is worth noting that the Gateway program has been recently put on an indefinite hold by NASA to concentrate financial and engineering resources on the establishment of a lunar surface base. Nevertheless, the trajectory optimization techniques and the orbital dynamics studied for this station remain highly relevant. The unique stability and coverage properties of the NRHO ensure that it will be utilized by future missions, keeping the study of these transfer maneuvers a crucial pillar for cislunar planning. [12]

2.3 Astrodynamic problem

As highlighted by the analysis of the Artemis program, the Lunar Gateway, and the CAPSTONE pathfinder mission, the sustainable return of humanity to the Moon requires a leap far beyond pure systems engineering. The hardware infrastructure outlined, composed of super-heavy launch vehicles, commercial landers, and habitation modules, represents only one side of the problem. The real operational challenge lies in the environment in which these systems must operate, cislunar space. Unlike low Earth orbits, this regime is governed by the complex and chaotic N-body gravitational interactions of the Earth–Moon–Sun system.

In this highly nonlinear environment, apparently stable nominal trajectories are subject to continuous dynamic perturbations, strict constraints, and inevitable navigation and maneuver execution uncertainties [8, 11, 6]. The dynamics analyzed in the previous sections demonstrate that the very survival of these missions is inseparably linked to astrodynamics. Whether it is computing the optimal placement of correction maneuvers for the Orion spacecraft while minimizing re-entry dispersion [8], or planning low-energy station-keeping and phase-change maneuvers to ensure a fifteen-year lifetime for the Gateway [11], classical Keplerian orbital mechanics is entirely insufficient.

To fly these missions within extremely limited propellant budgets and very tight error margins, space agencies must necessarily rely on increasingly advanced and robust numerical optimization and guidance strategies.

However, in order to understand, address, and solve these complex space optimization problems, it is first necessary to rigorously define the gravitational environment that generates them. Therefore, the dynamical reference models will be introduced, laying the theoretical foundations required for the study and subsequent simulation and numerical optimization of lunar trajectories.

Chapter 3

Astrodynamics

This chapter introduces the theoretical foundations and essential dynamical models for trajectory analysis in deep space and, in particular, in the cislunar environment. Since the dynamics in the vicinity of the Moon is dominated by a complex gravitational interaction among the Earth, the Moon, and the Sun, the classical Keplerian approximation proves limited and insufficient for planning modern space missions. Nevertheless, it is necessary to start from it in order to understand increasingly complete and representative models of the physical system in which we operate.

3.1 Two-Body Problem

The study of any space trajectory has its mathematical and conceptual starting point in the classical two-body problem. Although the cislunar environment in which modern exploration missions operate is governed by highly nonlinear N-body dynamics, a rigorous understanding of the two-body problem remains the fundamental prerequisite for defining nominal orbits and quantifying perturbation forces.

The two-body problem models the motion of two masses, m_1, the main attracting body, and m_2, the spacecraft, moving in empty space subject solely to their mutual gravitational attraction. Assuming a three-dimensional inertial reference frame, the absolute positions of the two bodies are defined by the vectors $\mathbf{R}_1$ and $\mathbf{R}_2$. In astrodynamics, however, the primary interest is not in the absolute motion in the universe, but rather in the motion of the satellite relative to the attracting body. We therefore define the relative position vector:

$$\mathbf{r} = \mathbf{R}_2 - \mathbf{R}_1 = r\hat{\mathbf{u}}_r \tag{3.1}$$

where r is the scalar distance and $\hat{\mathbf{u}}_r$ is the radial unit vector [13].

Applying Newton's second law of dynamics and the law of universal gravitation to each mass, and combining the respective differential equations, the vector equation of relative motion is obtained. Since the mass of the spacecraft m_2 is entirely negligible compared to the mass m_1, the sum $m_1 + m_2$ is approximated as m_1. The planetary gravitational parameter $\mu = Gm_1$ is thus introduced, where G is the universal gravitational constant. The fundamental equation of relative motion then takes its canonical form:

$$\ddot{\mathbf{r}} + \frac{\mu}{r^3}\mathbf{r} = \mathbf{0} \tag{3.2}$$

Equation 3.2 is a nonlinear second-order vector differential equation. Its analytical solution reveals the existence of constant vectors of motion that govern the entire geometry of trajectories in space.

The first fundamental constant is derived by computing the cross product between the position vector $\mathbf{r}$ and Equation 3.2. Since $\mathbf{r} \times \mathbf{r} = \mathbf{0}$, we obtain:

$$\mathbf{r} \times \ddot{\mathbf{r}} = \mathbf{0} \tag{3.3}$$

Recalling that the time derivative of the cross product $\mathbf{r} \times \dot{\mathbf{r}}$ equals $(\dot{\mathbf{r}} \times \dot{\mathbf{r}}) + (\mathbf{r} \times \ddot{\mathbf{r}})$, and that the first term vanishes as the cross product of parallel vectors, it is shown that the derivative of the specific angular momentum $\mathbf{h}$ is zero. Therefore:

$$\mathbf{h} = \mathbf{r} \times \mathbf{v} = \text{const.} \tag{3.4}$$

The fact that $\mathbf{h}$ is a constant vector has a crucial physical consequence: the position vector $\mathbf{r}$ and velocity vector $\mathbf{v}$ of the satellite always lie in the same plane, whose normal axis is defined by $\mathbf{h}$ itself. The unperturbed orbital motion is therefore strictly confined to a two-dimensional plane fixed in inertial space.

To determine the geometric equation of the trajectory, Equation 3.2 is cross-multiplied by the angular momentum $\mathbf{h}$ and then integrated with respect to time. The integration yields a constant vector of integration $\mathbf{C}$. Dividing this vector by μ, the eccentricity vector $\mathbf{e}$ is defined, a dimensionless parameter that lies in the orbital plane and points constantly toward the periapsis. The resulting vector relation is:

$$\frac{\mathbf{r}}{r} + \mathbf{e} = \frac{\mathbf{v} \times \mathbf{h}}{\mu} \tag{3.5}$$

To obtain a scalar expression, Equation 3.5 is projected along the position vector by taking the dot product of both sides with $\mathbf{r}$. Exploiting the scalar triple product identity $\mathbf{r} \cdot (\mathbf{v} \times \mathbf{h}) = (\mathbf{r} \times \mathbf{v}) \cdot \mathbf{h} = h^2$, the equation reduces to:

$$r + re\cos\theta = \frac{h^2}{\mu} \tag{3.6}$$

From which the well-known polar equation of the orbit is derived (Kepler's First Law):

$$r = \frac{h^2/\mu}{1 + e\cos\theta} \tag{3.7}$$

In this equation, θ represents the true anomaly, i.e., the angle measured from the line of apsides, the direction of the eccentricity vector, to the current position vector of the spacecraft. The magnitude of the eccentricity vector, e, uniquely determines the type of conic section: a circular orbit ($e = 0$), elliptic ($0 < e < 1$), parabolic ($e = 1$), or hyperbolic ($e > 1$).

A second fundamental conservation law is derived by taking the dot product of Equation 3.2 with the velocity vector $\dot{\mathbf{r}}$. Time integration of this relation yields the conservation equation of the specific mechanical energy, known as the vis-viva equation:

$$\varepsilon = \frac{v^2}{2} - \frac{\mu}{r} = \text{constant} \tag{3.8}$$

The specific orbital energy ε, the sum of kinetic and gravitational potential energy, remains constant along the entire trajectory and can only change due to external propulsive forces, such as the ΔV provided by the vehicle's engines [13]. For closed elliptic orbits ($e < 1$), the specific energy is negative and depends solely on the size of the semi-major axis a of the conic, according to the relation:

$$\varepsilon = -\frac{\mu}{2a} \tag{3.9}$$

Combining the previous equations, the energy equation is usefully expressed as:

$$\frac{v^2}{2} - \frac{\mu}{r} = -\frac{\mu}{2a} \tag{3.10}$$

The solid formalism of the Keplerian equations just derived is the tool of choice for designing astrodynamics in LEO or for computing first-approximation interplanetary trajectories based on the Patched Conics assumption [13, 14].

However, the ideal two-body model diverges drastically from physical reality as soon as the vehicle moves sufficiently far from Earth to feel the lunar gravitational pull. When computing trajectories for missions directed to the Lunar Gateway in NRHO, the lunar gravitational sphere of influence extends over 66,000 km. In this vast region, and near the Lagrangian libration points, the gravitational acceleration exerted by the Earth ($\mu_\oplus/r_1^2$) becomes of the same order of magnitude as that exerted by the Moon (μ_{Moon}/r_2^2).

The fundamental assumption of Equation 3.2, namely, the presence of a single dominant attractor, breaks down. This intrinsic limitation requires the adoption of a higher-order mathematical framework, the Circular Restricted Three-Body Model, which will be the subject of the following theoretical treatment of the cislunar environment.

3.2 Circular Restricted Three-Body Problem

Before introducing the equations governing the motion of a spacecraft in the cislunar environment, it is appropriate to define the characteristics of the Earth-Moon binary system. Although simplified models are used for analytical derivations, the real Earth-Moon system is characterized by complex orbital and rotational dynamics.

Assuming a mean Earth radius $R_\oplus = 6371$ km and a mean lunar radius $R_\mathbb{C} = 1734$ km, the dimensional ratio between the two bodies is approximately $R_\mathbb{C}/R_\oplus \simeq 1/4$. From a gravitational standpoint, considering $\mu_\oplus = 398600\ \mathrm{km}^3/\mathrm{s}^2$ and $\mu_\mathbb{C} = 4904\ \mathrm{km}^3/\mathrm{s}^2$, the mass ratio is $\mu_\mathbb{C}/\mu_\oplus \simeq 1/81.4$. These parameters place the barycenter of the system at a distance x from the center of the Earth equal to:

$$x = \frac{\mu_\mathbb{C}}{\mu_\mathbb{C} + \mu_\oplus} R = \frac{R}{1 + \frac{\mu_\oplus}{\mu_\mathbb{C}}} = \frac{384400}{1 + 81.4} \simeq 4671 \text{ km} \tag{3.11}$$

where R is the mean Earth-Moon distance. Since the Earth's radius is greater than 4671 km, the system's barycenter is physically located inside the Earth.

The real orbit of the Moon is subject to continuous variations. The orbital eccentricity oscillates around a mean value of $e \simeq 0.055$, ranging from 0.044 to 0.059 due to solar perturbations. Furthermore, the line of apsides, connecting perigee and apogee, undergoes precession, rotating by 3° per revolution and completing a full cycle in 8.85 years. Added to this are librations, related to the inclination of the lunar rotation axis of 6.68° with respect to the normal to the ecliptic, and tidal effects. The tidal interaction causes a slowdown of Earth's rotation of approximately 1.46 m/s per century, which translates, by conservation of the system's angular momentum, into a progressive recession of the Moon of approximately 3.8 cm per year. All these real ephemerides are tracked and made available by high-precision systems such as JPL Horizons [15, 16].

To mathematically model the trajectories of a spacecraft within this perturbed system, the CR3BP is introduced. Astrodynamics relies on three fundamental assumptions:

1. **3-Body Problem:** The system consists exclusively of two primary masses, e.g., Earth and Moon, and a third body, the spacecraft.
2. **Restricted Problem:** The mass of the spacecraft m is infinitely smaller than those of the primaries ($m \ll m_1, m_2$). As a consequence, the spacecraft exerts no gravitational influence on the motion of m_1 and m_2.
3. **Circular Problem:** The two primary bodies are assumed to move on perfectly circular orbits around their common center of mass.

Defining the total mass of the system as $M = m_1 + m_2$, the dimensionless mass parameter $\mu = \frac{m_2}{M}$ is introduced, where m_2 belongs to the less massive body. In the Earth-Moon system, this parameter takes the value $\mu \simeq 0.0125$. The masses of the primaries can then be expressed as functions of M and μ as $m_2 = \mu M$ and $m_1 = (1-\mu)M$.

To remove the time dependence associated with the revolution of the primaries, a synodic rotating reference frame centered at the system's barycenter is adopted. The frame rotates with constant angular velocity $\bar{\omega} = [0, 0, \omega]^T$ perpendicular to the orbital plane. The positions of the two primaries along the x-axis are fixed and equal to $-\mu R$ and $(1-\mu)R$, respectively [15, 16].

Let $\bar{r}$ be the absolute position vector of the spacecraft in the inertial reference frame. As in Section 3.1, Newton's Second Law states that the absolute acceleration is generated by the sum of the gravitational attraction forces $\bar{F}_1$ and $\bar{F}_2$ exerted by the two primaries:

$$\bar{a}_{abs} = \frac{\bar{F}_1 + \bar{F}_2}{m} = -G\frac{m_1 m}{r_1^3}\bar{r}_1 - G\frac{m_2 m}{r_2^3}\bar{r}_2 \tag{3.12}$$

where $\bar{r}_1$ and $\bar{r}_2$ denote the position vectors of the satellite with respect to the two primaries. Applying the Transport Theorem to express the acceleration in components of the rotating frame, fictitious terms arising from the relative kinematics appear:

$$\ddot{\bar{r}} + \bar{\omega} \wedge (\bar{\omega} \wedge \bar{r}) + 2\bar{\omega} \wedge \dot{\bar{r}} = \frac{1}{m}(\bar{F}_1 + \bar{F}_2) \tag{3.13}$$

In this formulation, $\ddot{\bar{r}}$ is the relative acceleration, $\bar{\omega} \wedge (\bar{\omega} \wedge \bar{r})$ represents the centripetal acceleration, and $2\bar{\omega} \wedge \dot{\bar{r}}$ is the Coriolis acceleration.

Expanding the Cartesian components (x, y, z), the system of dimensional differential equations is obtained. To generalize the problem and improve the numerical stability of integrations, the equations are made dimensionless. The dimensionless spatial variables $\xi = x/R$, $\eta = y/R$, $\zeta = z/R$, represented by the vector $\bar{\rho}$, and a dimensionless time variable $\tau = t\omega$ are introduced. Substituting the definitions of the masses relative to the parameter μ, the standard canonical form of the equations of motion for the CR3BP is obtained [15, 16]:

$$\xi'' - 2\eta' - \xi = -(1-\mu)\frac{\xi + \mu}{\rho_1^3} - \mu\frac{\xi - (1-\mu)}{\rho_2^3} \tag{3.14a}$$

$$\eta'' + 2\xi' - \eta = -(1-\mu)\frac{\eta}{\rho_1^3} - \mu\frac{\eta}{\rho_2^3} \tag{3.14b}$$

$$\zeta'' = -(1-\mu)\frac{\zeta}{\rho_1^3} - \mu\frac{\zeta}{\rho_2^3} \tag{3.14c}$$

where primes denote derivatives with respect to the dimensionless time τ, and the terms $\rho_1 = \sqrt{(\xi+\mu)^2 + \eta^2 + \zeta^2}$ and $\rho_2 = \sqrt{(\xi - (1-\mu))^2 + \eta^2 + \zeta^2}$ denote the dimensionless distances of the vehicle from the primaries.

The equations just derived (3.14) can be expressed in a more compact form by grouping the gravitational effect of the primaries and the centrifugal acceleration, the linear terms ξ and η, into a single scalar function defined as the pseudo-potential $\mathcal{U}$:

$$\mathcal{U} = \frac{1-\mu}{\rho_1} + \frac{\mu}{\rho_2} + \frac{1}{2}(\xi^2 + \eta^2) \tag{3.15}$$

Computing the partial derivatives of the pseudo-potential with respect to ξ, η, and ζ, the vector system of motion condenses to:

$$\ddot{\bar{\rho}} + 2\bar{\omega} \wedge \dot{\bar{\rho}} = \nabla \mathcal{U} \tag{3.16}$$

Of particular astrodynamic interest are the points where both accelerations and velocities in the rotating frame are zero ($\dot{\bar{\rho}} = \ddot{\bar{\rho}} = 0$). At these positions, gravitational forces and centrifugal acceleration perfectly balance, allowing a theoretical satellite to maintain its position fixed relative to the Earth and Moon. This equilibrium condition implies $\nabla \mathcal{U} = 0$.

Since the derivative along the ζ axis imposes:

$$\frac{\partial \mathcal{U}}{\partial \zeta} = -\zeta \left(\frac{1-\mu}{\rho_1^3} + \frac{\mu}{\rho_2^3} \right) = 0 \tag{3.17}$$

the only possible solution is $\zeta = 0$, demonstrating that all equilibrium points lie entirely in the orbital plane of the primaries ξ, η. Solving the in-plane derivatives, five solutions emerge, known as Lagrangian Points:

- Collinear Points (L_1, L_2, L_3): Located on the axis joining the primaries ($\eta = 0$).
  - L_1 (*Cis-lunar point*): Located between the two masses ($-\mu < \xi < 1-\mu$). Distance from the smaller body approximated as $\rho_2 \simeq \sqrt[3]{\mu/3}$, approximately 61500 km from the Moon.
  - L_2 (*Trans-lunar point*): Located beyond the smaller mass body ($\xi > 1-\mu$). Also at a distance from the smaller body of approximately $\rho_2 \simeq \sqrt[3]{\mu/3}$.
  - L_3 (*Trans-earth point*): Located beyond the more massive body ($\xi < -\mu$). Its distances are approximated as $\rho_1 \simeq 1$ and $\rho_2 \simeq 2$ [15].
- Equilateral Points (L_4, L_5): They share the same distance from both primaries, namely $\rho_1 = \rho_2 = 1$. Their exact dimensionless coordinates are $\xi = \frac{1}{2} - \mu$ and $\eta = \pm\frac{\sqrt{3}}{2}$, forming equilateral triangles with the primary masses.

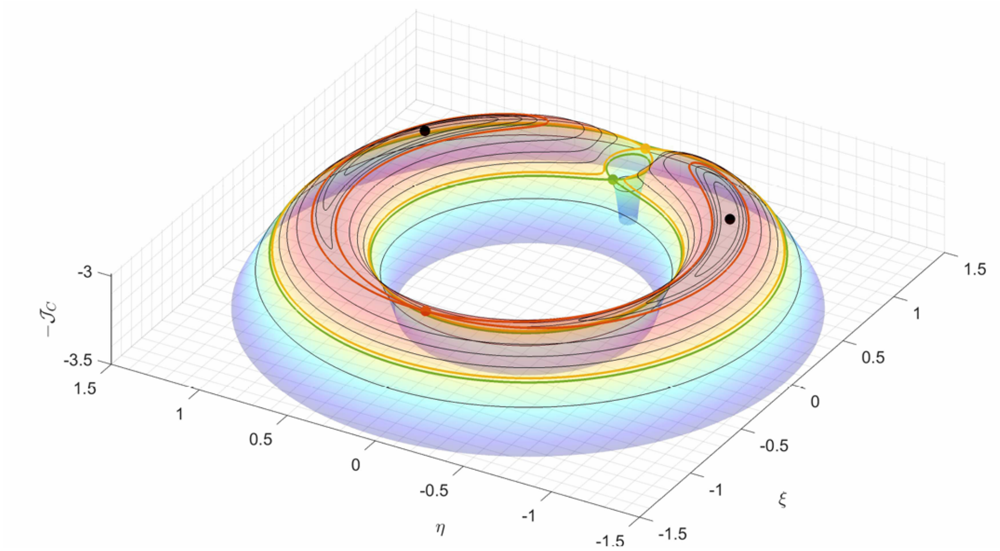

Figure 3.1: Representation of Jacobi constant and Lagrangian Points in the synodic frame [16].

Multiplying the equation of motion expressed as a gradient by the velocity vector $\dot{\bar{\rho}}$ and integrating with respect to the dimensionless time τ, the Coriolis term vanishes due to the orthogonal cross product. The result of this operation yields the only constant of motion in the CR3BP, the Jacobi Integral:

$$\frac{1}{2}\frac{dV^2}{d\tau} = \frac{d\mathcal{U}}{d\tau} \quad \Rightarrow \quad V^2 = 2\mathcal{U} - C \tag{3.18}$$

where V is the magnitude of the velocity in the rotating frame and C is called the Jacobi Constant. This constant defines the energy level of the satellite as a function of its initial conditions.

Since the relative kinetic energy, i.e., the squared quantity V^2, must be intrinsically positive for motion to physically exist ($V^2 > 0$), the geometric space accessible to the spacecraft is constrained by the inequality:

$$2\mathcal{U} - C \geq 0 \quad \Rightarrow \quad C \leq 2\mathcal{U} \tag{3.19}$$

The boundary of this inequality, obtained by setting the satellite's velocity to zero ($2\mathcal{U} - C = 0$), generates a geometric locus in three-dimensional space known as Zero Velocity Surfaces or Hill Surfaces. These surfaces define a clear separation between the regions of space where satellite motion is possible and the forbidden regions [15, 16].

The topology of these surfaces depends strictly on the value of the Jacobi Constant. In the Earth-Moon system, as the energy of the spacecraft decreases, i.e., for increasing values of the constant C, the accessible regions of space shrink until they close and isolate the two primaries. The contact points and the progressive opening or closing of the "bottlenecks" between the different accessible zones coincide exactly with the Lagrangian Points. Each Lagrangian point is associated with a specific energy level.

3.3 Stable Orbits in CR3BP

It is possible to visualize the solutions of the CR3BP in purely geometric terms. Unlike the two-body problem, where closed orbits are limited to perfect ellipses and circles, the CR3BP hosts an infinite variety of periodic trajectories with complex and fascinating shapes. To study their characteristics and exploit them in space missions, these trajectories are classified into continuous families, whose members share similar dynamical properties but vary in size and energy level.

3.3.1 Classification of periodic orbits

The classification of the numerous periodic orbits in the Earth-Moon system is based on two main geometric criteria. The first criterion distinguishes between planar orbits and three-dimensional orbits. Planar orbits lie entirely in the revolution plane of the two primary bodies ($z = 0$), limiting the motion to only two spatial degrees of freedom. Three-dimensional orbits, on the other hand, exhibit a significant excursion out of the system's equatorial plane, exploiting the z component to generate complex spatial trajectories.

The second classification criterion concerns the geometric center around which the spacecraft orbits. A distinction is thus made between Libration Point Orbits (LPOs), trajectories that oscillate around the Lagrangian equilibrium points, typically the collinear points L_1 and L_2, and orbits around the primaries, which physically surround the Earth or the Moon. A well-known example of the latter are the Distant Retrograde Orbits, highly stable planar orbits in which the vehicle revolves around the Moon in the direction opposite to the lunar motion. In the context of this work, the focus will be on the LPOs associated with the collinear points [17, 18].

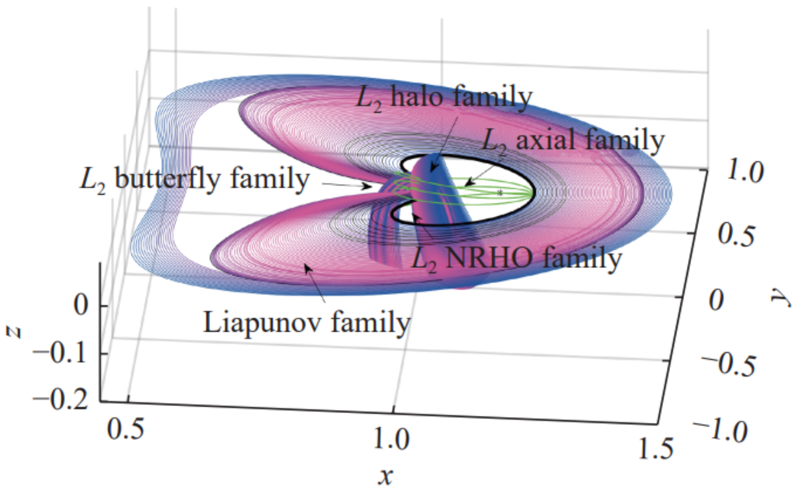

Figure 3.2: Spatial representation of several families of periodic orbits in the Earth-Moon system.[18].

3.3.2 Lyapunov Planar Orbits

Lyapunov orbits represent the fundamental family of planar periodic orbits associated with the collinear points L_1, L_2, and L_3. Since they lie strictly in the lunar ecliptic plane $x - y$, their dynamics are the simplest to study within the LPOs [18].

For energy levels very close to those of the reference Lagrangian point, i.e., for high values of the Jacobi Constant, Lyapunov orbits appear as small ellipses centered exactly at the libration point. However, as energy is added to the system and the Jacobi Constant decreases, these orbits expand away from the Lagrangian point and approach the primary bodies. Due to the strong nonlinearity of the lunar gravitational field, the shape of these trajectories progressively distorts, from regular ovals, they transform until they take on a characteristic bean or crescent shape, bending toward the gravitational well of the smaller body [16].

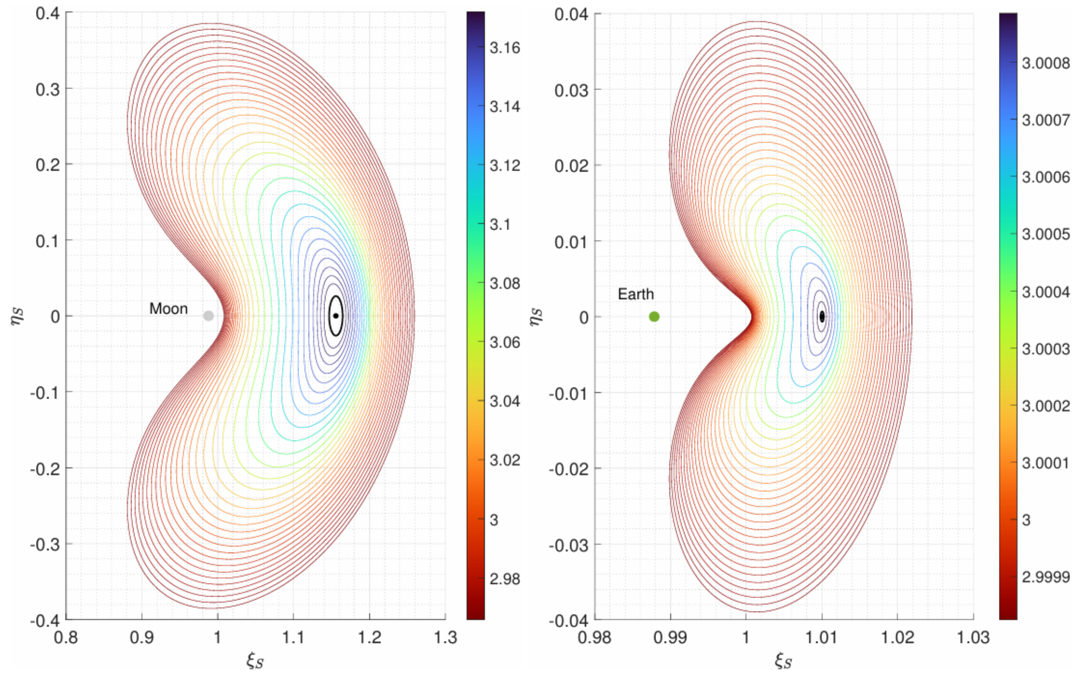

Figure 3.3: Family of planar Lyapunov orbits around the point L_2 of the Earth-Moon system[16].

3.3.3 Halo Orbits and bifurcations

Halo orbits constitute one of the most well-known and widely used three-dimensional families for deep space missions. Their origin is intrinsically linked to the evolution of planar orbits. As a Lyapunov orbit grows in amplitude, the oscillation frequency in the $x - y$ plane can synchronize with the natural oscillation frequency along the vertical z axis.

When these two frequencies enter resonance, a mathematical phenomenon known as bifurcation occurs, the planar family breaks and generates a new family of orbits that extend into three-dimensional space. The Halo orbits arising from this bifurcation lose symmetry with respect to the equatorial plane, but maintain a mirror symmetry with each other. Two distinct branches are always generated: the Northern Halo, with maximum excursion toward the North of the system, and the Southern Halo, with maximum excursion toward the South. Thanks to their pronounced three-dimensionality, Halo orbits around L_1 or L_2 allow both the Earth and the polar regions of the Moon to be kept constantly in view, making them ideal for telecommunication satellites [18].

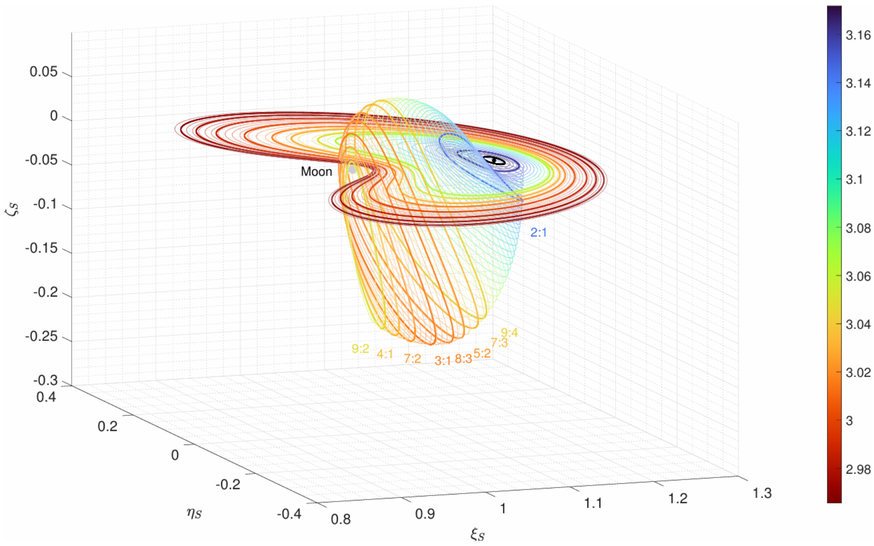

Figure 3.4: Three-dimensional visualization of the bifurcation: The Halo family of orbits arises and develops in 3D space, breaking away from the underlying planar Lyapunov family[16].

3.3.4 Near Rectilinear Halo Orbits

Within the broad family of Halo orbits, there exists a highly specialized subset that has recently revolutionized cislunar exploration planning: the Near Rectilinear Halo Orbits. Geometrically, these are extremely elongated Halo orbits that, when observed from the rotating frame, appear almost as vertical straight lines. Along these trajectories, the spacecraft passes very close to one of the lunar poles at periapsis, before extending deeply into space at apoapsis.

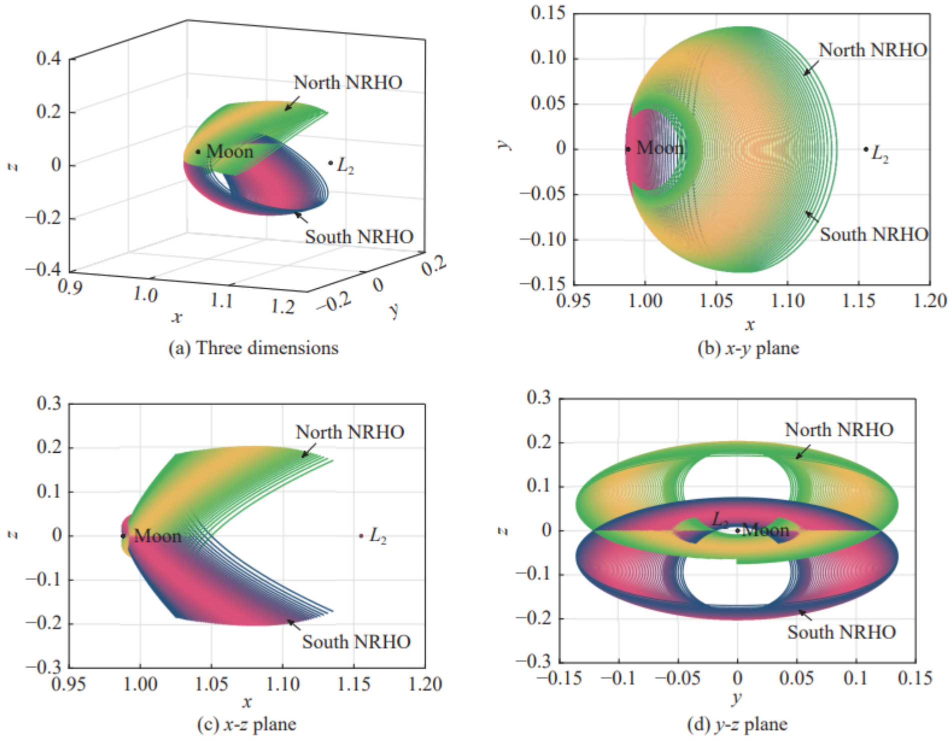

Figure 3.5: Representation of the NRHO family [18]

The fundamental engineering characteristic of NRHOs is their exceptional linear stability. While standard Halo and Lyapunov orbits are chaotic and highly unstable in a real system, requiring continuous and costly corrective maneuvers, NRHOs are intrinsically far more stable. As a result, the propulsive cost to maintain a vehicle on an NRHO is almost negligible [19].

Furthermore, NRHOs can be designed to exploit specific synodic resonances with the Moon. The 9:2 resonance, in which the vehicle completes 9 revolutions for every 2 lunar synodic months, has been selected by NASA and its international partners as the destination orbit for the Lunar Orbital Platform-Gateway. This specific southern NRHO trajectory ensures energetically inexpensive access to the lunar surface, continuous line-of-sight communication with the Earth, and, most importantly, guarantees the complete absence of Earth or lunar eclipses for years, a vital requirement for solar power generation and thermal management of the crewed outpost [18, 19].

3.4 N-Body Problem

The astrodynamic analysis conducted through the Two-Body Problem and the CR3BP provides the fundamental theoretical basis for understanding cislunar orbits. However, in the real scenario of spaceflight, a vehicle is never subject solely to the attraction of one or two ideal attractors. To accurately model the trajectories of missions such as Artemis or the Lunar Gateway, it is necessary to abandon the simplifying assumptions and formulate the motion through the N-Body Problem.

The N-body problem studies the dynamics of a system consisting of N point masses $m_1, \dots, m_N$ that mutually attract each other in a vacuum according to the law of universal gravitation, with no geometric restrictions or mass hierarchies. Given an inertial reference frame in $\mathbb{R}^3$, let $x_j \in \mathbb{R}^3$ be the position vector of the j-th mass. Newton's differential equations of motion form a coupled second-order system of dimension $3N$, described by:

$$m_j \ddot{x}_j = \sum_{k \neq j} m_j m_k \frac{x_k - x_j}{||x_k - x_j||^3} \quad \text{for } j = 1, \dots, N \tag{3.20}$$

The analytical solution of the N-body problem represents one of the greatest challenges of classical mechanics. The only constants of motion always valid for an isolated N-body system are energy, total linear momentum, global angular momentum, and the position of the barycenter. At the end of the 19th century, H. Bruns and P. Painlevé proved that no other independent algebraic first integrals exist, while H. Poincaré, with his celebrated impossibility theorem, definitively established the non-existence of further non-trivial uniform analytic first integrals for $N \geq 3$. This intrinsic dynamical non-integrability, related to resonance phenomena and small denominators in the development of perturbative series, makes it impossible to find an exact closed-form solution.

For these reasons, the quantitative study of the N-body problem must inevitably and exclusively rely on numerical integration of the differential equations [20].

The necessity of using numerical solvers opens the door to the use of so-called N-body ephemeris models. In these high-fidelity computational environments, the positions of the perturbing celestial bodies, such as the Sun, the Earth, and the planets, do not derive from simplified equations, but are extracted at each time step from highly accurate databases, such as the NASA/JPL SPICE libraries.

When analyzing the trajectory of a vehicle orbiting, for example, around the Lunar Gateway in such a regime, third-body perturbations dominate the scenario. A vehicle in an NRHO is not subject only to the basic gravitational interaction of the Earth and Moon, but is heavily influenced by solar gravity. Added to this are complex perturbations such as solar radiation pressure and the irregularity of the lunar gravitational field, when modeled not as a point mass but through spherical harmonics models.

In this asymmetric and chaotic dynamical environment, the CR3BP theory undergoes a profound geometric transformation. The NRHOs, which in the restricted model are strictly and perfectly periodic orbits, lose their closed nature and become quasi-periodic orbits. The trajectory of the vehicle in space never perfectly overlaps the previous revolution, oscillating continuously within a toroidal manifold.

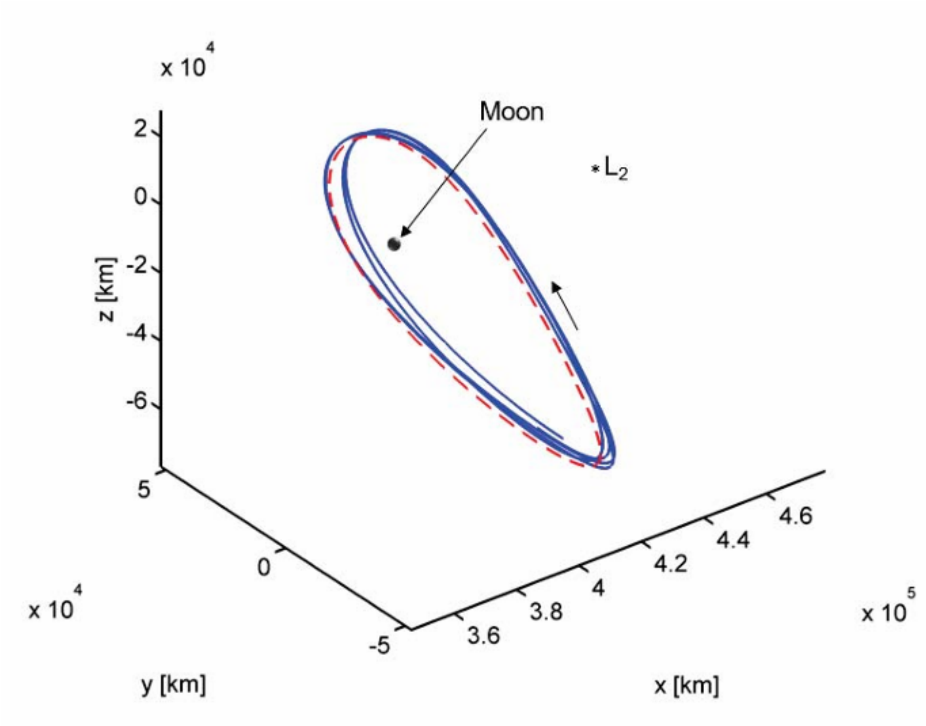

Figure 3.6: Transition of four revolutions of a CR3BP L2 halo orbit (red dashed) to an ephemeris model (blue solid) [21].

This quasi-periodicity, combined with the intrinsically nonlinear nature of the N-body system and operational navigation errors, means that any object left to drift in an NRHO will inevitably depart from it within a relatively short time, typically between 30 and 100 days for uncontrolled vehicles, depending on the perturbations. For the long-term survival of missions such as the Gateway, it is therefore essential not only to rely on computers to propagate orbits in time, but also to continuously implement periodic station-keeping maneuvers to counteract the natural instability and confine the vehicle within the safe envelope of its nominal quasi-periodic orbit [22].

Chapter 4

Trajectory Optimisation

The design of space missions, particularly those directed toward the cislunar environment or deep space, requires meticulous planning to maximise mission effectiveness while operating within strict physical and technological constraints. Trajectory optimisation is the mathematical and engineering discipline concerned with determining the optimal path for a spacecraft, minimising or maximising a specific performance index, such as propellant consumption or flight time, while satisfying the equations of dynamics and operational constraints [23].

4.1 Optimisation Methods

Mathematically, the problem of optimising a space trajectory is formulated as an Optimal Control Problem. The objective is to determine a time history of the control vector $u(t)$ and the state vector $x(t)$ that minimises a cost function J, typically expressed in the Bolza form [24]:

$$J(\mathbf{x}, \mathbf{u}, t) = \phi(\mathbf{x}(t_f), t_f) + \int_{t_0}^{t_f} g(\mathbf{x}(t), \mathbf{u}(t), t)\, dt \tag{4.1}$$

where ϕ represents the terminal cost (Mayer term), and g represents the cost distributed along the trajectory (Lagrange term), such as the integral of acceleration to minimise propellant consumption.

Due to the strong nonlinearities of orbital mechanics, especially in the N-body problem, closed-form analytical solutions are impossible to obtain, making the use of numerical approaches necessary. Numerical methods for solving OCPs are divided into three main families:

- **Indirect Methods:** Based on the Pontryagin Maximum Principle, they transform the optimisation problem into a boundary value problem. They offer very high analytical precision, but exhibit convergence that is extremely sensitive to the initial guess of the co-states, which are non-physical variables that are difficult to estimate.

- **Direct Methods:** They discretise the time history of states and controls, transforming the infinite-dimensional OCP into a finite-dimensional Nonlinear Programming problem. They are much more robust with respect to initial guesses and handle path constraints easily, but introduce approximations due to discretisation.
- **Stochastic Methods:** Gradient-free global search algorithms that explore the entire solution space without requiring the computation of derivatives. They are immune to local minima and do not require an initial guess, but have high computational costs and do not guarantee exact first-order optimality.

[23, 24, 25]

4.2 Genetic Algorithm

Among the stochastic methods applied to astrodynamics, Genetic Algorithms have established themselves as one of the most powerful mathematical and computational tools for global exploration of the trajectory design space. Belonging to the family of Evolutionary Computation, GAs are inspired by the biological principles of Darwinian evolution and natural selection. Unlike deterministic methods based on differential calculus, such as indirect techniques or SQP nonlinear programming methods, GAs operate on a population of individuals, each representing a candidate trajectory, i.e., a candidate solution to the optimal control problem.

The fundamental characteristic that makes GAs indispensable for optimising complex trajectories in cislunar space, such as transfers to NRHO orbits, lies in their gradient-free nature. The algorithm does not require the computation of objective function derivatives or a user-provided initial guess. Operating probabilistically, the GA is able to navigate highly non-convex, discontinuous fitness landscapes populated by countless local minima [26, 27].

4.2.1 Encoding

The first mathematical step in constructing a GA is defining the mapping between the physical problem space and the genetic space of the algorithm. The independent characteristics of each trajectory, such as departure epochs, flight times, ΔV magnitudes, or angular variables, constitute the design variables and are identified as the genes of the individual. The collection of all genes forms the chromosome or genotype, which uniquely describes an individual in the population.

In the first generation of GAs, Binary Encoding was used, in which continuous variables were discretised into strings of 1s and 0s. For example, a variable bounded within $[x_L, x_U]$ was discretised with a resolution r_i depending on the number of bits b_i:

$$r_i = \frac{x_U - x_L}{2^{b_i} - 1} \tag{4.2}$$

However, astrodynamics requires very high precision. Using binary encoding to achieve tolerances on the order of centimetres or millimetres per second would result in intractable chromosome lengths. Therefore, modern orbital optimisers implement Real Encoding, in which each gene is represented directly by its floating-point value. This paradigm not only eliminates discretisation errors, but also drastically improves the convergence properties of the algorithm in continuous spaces [27].

4.2.2 Fitness and Penalty Functions

Classic GAs are designed to solve unconstrained optimisation problems. However, an orbital transfer problem is intrinsically constrained by the N-body equations of dynamics and by strict operational limits, e.g., minimum perigee altitude, maximum characteristic energy C_3, limits on available ΔV. To allow the GA to handle constraints, the Penalty Functions method is employed, which transforms the original problem into an unconstrained one.

The original objective function $J(w)$, such as propellant consumption ΔV, is combined with penalty terms associated with each constraint violation to form the fitness function $F(w)$, which the algorithm must minimise:

$$F(\mathbf{w}) = WJ(w) + \sum_{k=1}^{N_p} W_k P_k(w) \tag{4.3}$$

where W is the weight associated with the primary objective, N_p is the total number of constraints considered, $P_k(w)$ is the magnitude of the violation of the k-th constraint, and W_k is the corresponding penalty weight [28, 26].

Tuning the weights W_k is a critical aspect:

- If the penalty is too severe, the GA will immediately discard any infeasible solution, making the exploration blind and turning the fitness landscape into a discontinuous map dominated by artificial minima. Infeasible individuals that carry valuable genetic material would be lost.

- If the penalty is too mild, the population will converge toward solutions with excellent propellant consumption but that are physically unfeasible, e.g., trajectories that intersect the surface of a planet.

4.2.3 Genetic Operators

The evolution of the population, generation after generation, is governed by the stochastic yet systematic application of specific mathematical operators: Selection, Crossover, Mutation, and Elitism. The balance among these operators defines the trade-off between Exploitation of promising areas and Exploration of new regions.

The selection operator extracts individuals from the current population to form the mating pool. The objective is to favour the survival of individuals with the best fitness, inducing selective pressure on the population. Several mathematical strategies can be adopted:

1. **Fitness Proportionate Selection (FPS):** The probability of selecting an individual is strictly proportional to its fitness relative to the population mean. In the early stages of optimisation, this method causes premature takeover: the few decent individuals immediately dominate selection, blocking exploration and causing convergence to local minima.

2. **Sigma Scaling:** Improves FPS by scaling the fitness based on the standard deviation σ of the population. This mitigates selective pressure in the early stages, when σ is high, and increases it in the later stages, when σ is low and individuals are very similar, keeping the evolution active.

3. **Tournament Selection:** This is the preferred method for trajectory optimisation. A limited number of individuals is randomly drawn from the population and made to compete. The individual with the best fitness wins the tournament with a probability $r \in [0.7, 0.9]$ and is passed to the mating pool. This method is computationally very fast, maintains a constant and easily controllable selective pressure through r, and occasionally allows weaker solutions to survive, ensuring global exploration.

The crossover operator is the main engine through which the algorithm explores the solution space, directly inspired by biological reproduction. This operator selects promising trajectories, the parents, from the mating pool and mixes their mission parameters, the genes, to generate new child trajectories.

The fundamental objective of crossover is to combine the optimal characteristics discovered by the population up to that point. In astrodynamic terms, if one parent trajectory has a very efficient departure manoeuvre and the other has an excellent arrival geometry, combining their parameters offers the possibility of generating a child trajectory that inherits both advantages.

In modern real-encoded implementations, crossover does not simply swap values but blends parameters proportionally to their distance. This creates a very useful adaptive behaviour: in the early stages of optimisation, when the population trajectories are very different from one another, crossover generates children scattered in new regions of the space, favouring global exploration. As the population evolves and concentrates in a promising region, parents become similar to each other. As a result, crossover begins to generate children in the immediate proximity, effectively performing local refinement of the trajectory.

While crossover combines information already present in the population, the mutation operator has the crucial task of introducing entirely new and random genetic material into the system. Applied with a typically very low probability, mutation consists of stochastically altering one or more parameters of a single newly generated trajectory. In the context of orbital optimisation, this translates into small random perturbations, such as a slight change in a ΔV component or a small shift in the epoch of a manoeuvre. The vital function of mutation is to prevent genetic stagnation and premature convergence. Without this operator, selective pressure would rapidly drive the entire population to become identical to the first sub-optimal trajectory found, trapping the algorithm in a local minimum. By continuously introducing random perturbations, mutation perturbs the trajectories, forcing the algorithm to continuously probe the boundaries of the search space and ensuring that the genetic diversity of the population remains alive until the true global minimum is discovered.

Due to the stochastic nature of crossover and mutation, there is always a statistical risk that the best trajectory found up to a given point in the optimisation is destroyed. Elitism addresses this problem by taking a small fixed fraction, typically 5–7%, of the best individuals from the current generation and injecting them unchanged and protected into the next generation, replacing the worst newly created individuals. This operator guarantees the monotonicity of the asymptotic convergence of the fitness [27].

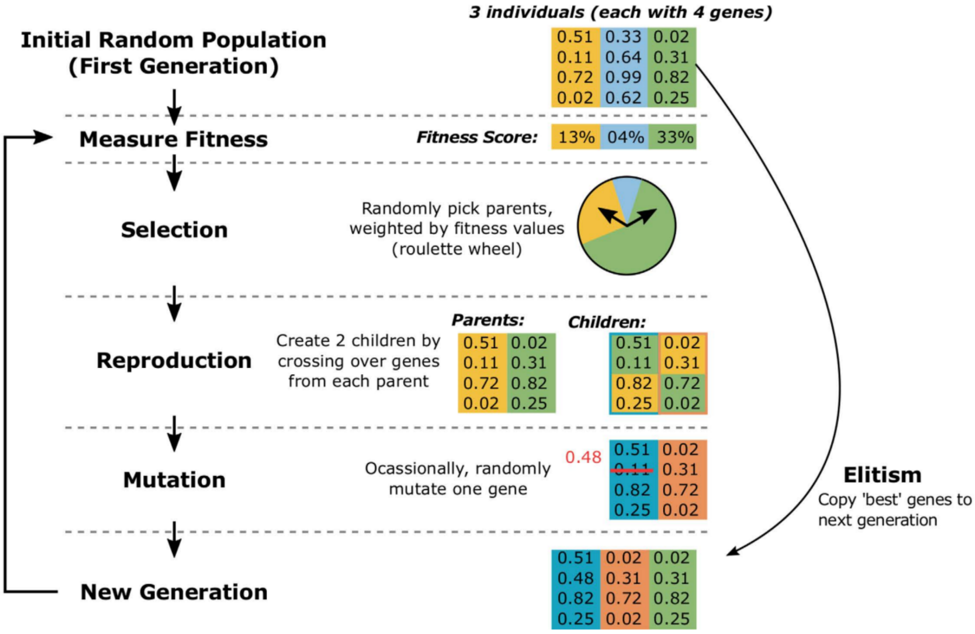

Figure 4.1: GA flow chart [29].

4.2.4 Evolution of Gene Distribution and GA Behaviour

The effectiveness of the global search of a GA can be demonstrated by statistically analysing the spatial distribution of genes across generations. In an n-dimensional astrodynamic design space, the initial population is dispersed according to a uniform distribution, analogous to white noise. This dispersion guarantees the absence of bias and forces the system to globally probe the entire hypercubic volume of the domain $\mathbb{R}^n$.

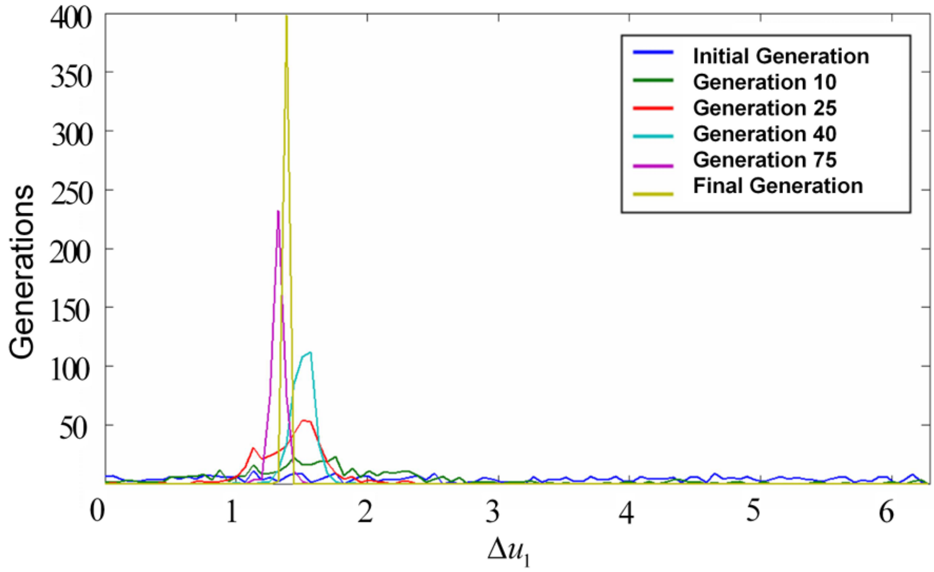

Figure 4.2: Evolution of the distribution of a single design variable across the generations of a Genetic Algorithm [27].

Under the continuous action of selective pressure, successive generations witness a massive clustering of individuals toward the valleys of minimum fitness. Mathematically, the probability density of the genes changes shape, taking on a Gaussian profile centred on the most promising attraction basins.

Toward the end of the optimisation process, the variance of the population collapses. All trajectories in the algorithm converge in an infinitesimal region around the best estimate of the global minimum, and the gene distribution takes on the limiting behaviour of a Dirac delta [27]. It is precisely at this point that the genetic algorithm exhausts its potential: the lack of genetic diversity prevents any further significant improvement, producing a solution that, although globally centred in the correct basin, is rough and lacks convergence to the exact tolerances required by a high-fidelity model. This intrinsic limitation justifies and makes imperative the extraction of the elite individual and its transfer to a deterministic local refinement stage.

4.3 Sequential Quadratic Programming

While GAs perform exploratory global-scale search by moving stochastically, they prove imprecise when it comes to refining the details of a trajectory to satisfy strict physical tolerances, such as the exact orbital insertion altitude. For this high-precision task, astrodynamics relies on deterministic methods, and in particular on the SQP algorithm. The SQP algorithm is the industry standard for space trajectory refinement, implemented in mission software such as NASA's MALTO or Copernicus [23, 28].

4.3.1 Direct Transcription

The first obstacle the numerical solver must face is the continuity of time. A real space trajectory is described by a system of continuous differential equations $\dot{\mathbf{x}}(t) = f(x(t), u(t), t)$. A computer cannot, however, manipulate an infinite-dimensional curve; it therefore resorts to Direct Transcription.

Through transcription, the algorithm fragments the trajectory into a sequence of N discrete time nodes, transforming the Optimal Control Problem into a large finite-dimensional numerical puzzle known as Nonlinear Programming. All physical states and propulsive controls at each node are concatenated into a single large optimisation variable vector $\mathbf{X} = [\mathbf{x}_1, \mathbf{u}_1, \ldots, \mathbf{x}_N, \mathbf{u}_N]^T$. The problem is then set up in its canonical form:

$$\min_{\mathbf{X}} \quad J(\mathbf{X}) \tag{4.4}$$

$$\text{subject to:} \quad \mathbf{h}(\mathbf{X}) = \mathbf{0}, \quad \mathbf{g}(\mathbf{X}) \leq \mathbf{0} \tag{4.5}$$

4.3.2 SQP Logic

The N-body gravitational environment generates a chaotic and highly nonlinear mathematical fitness landscape. To simultaneously balance the desire to save propellant and the obligation to respect the physics, the algorithm introduces the system's Lagrangian function $\mathcal{L}$:

$$\mathcal{L}(\mathbf{X}, \boldsymbol{\lambda}) = J(\mathbf{X}) + \boldsymbol{\lambda}^T \mathbf{h}(\mathbf{X}) \tag{4.6}$$

where the Lagrange multipliers $\boldsymbol{\lambda}$ act as a system of penalties for violations of the orbital dynamics.

Since computing the global minimum of this complex equation in a single step is impossible, the SQP algorithm applies a quadratic approximation. At each iteration k, the algorithm analyses the curvature around its current state $\mathbf{X}_k$ and assumes that the irregular landscape behaves locally like a perfect smooth parabolic bowl. Mathematically, this is achieved by expanding the Lagrangian in a Taylor series up to the second term to find the optimal step $\Delta\mathbf{X}$:

$$\mathcal{L}(\mathbf{X}_k + \Delta\mathbf{X}) \approx \mathcal{L}(\mathbf{X}_k) + \nabla\mathcal{L}^T \Delta\mathbf{X} + \frac{1}{2}\Delta\mathbf{X}^T \mathbf{H}_{\mathcal{L}} \Delta\mathbf{X} \tag{4.7}$$

Finding the exact bottom of a simple parabola is a nearly instantaneous computation. The algorithm moves to the bottom of this artificial bowl, recomputes the solution at the new point, constructs a new parabola, and repeats this quadratic programming sub-problem until it asymptotically converges to the bottom of the true valley [25, 23].

4.3.3 Line Search

This approximation, however, conceals a significant structural pitfall. Since the real problem is nonlinear, moving directly and fully in the direction dictated by the bottom of the parabola $\Delta \mathbf{X}_k$ could lead to a region of space where the true physical constraints are heavily violated, for example, crossing the lunar surface.

To mitigate this risk, SQP introduces a safety mechanism known as Line Search. The algorithm defines the new trajectory by scaling the step through a parameter $\alpha \in (0, 1]$:

$$\mathbf{X}_{k+1} = \mathbf{X}_k + \alpha \Delta \mathbf{X}_k \tag{4.8}$$

Rather than blindly jumping to the end of the step, the solver analyses the line traced by $\Delta \mathbf{X}_k$ and travels only a fraction of it, reducing α until the internal Merit Function confirms a genuine improvement of the trajectory without generating unacceptable residuals in the equations of motion.

This mathematical caution can, however, trigger the Maratos Effect. In the most critical and highly nonlinear regions, such as a close flyby where the Moon's gravitational field sharply curves space, the linear and parabolic projection computed by SQP becomes a poor approximation of reality. The solver identifies a direction that would dramatically reduce propellant consumption, but recognises that even an infinitesimally small step along that line would cause an uncontrollable jump in the dynamic constraint error. The Line Search module progressively reduces the step size, driving α to infinitesimal values and effectively freezing the trajectory in a sub-optimal state.

The Maratos Effect mathematically demonstrates the intrinsic global blindness of deterministic methods based on differential calculus. For the SQP algorithm to exploit its speed and local accuracy, hybridisation becomes mandatory: the SQP must operate starting from an initial guess provided by a global stochastic explorer that has already conducted a global search within the correct solution basin [28, 26, 25].

4.4 Hybrid Approach

Exploring the N-body cislunar environment presents an extremely hostile fitness landscape, jagged, discontinuous, and populated by countless local minima. As analysed in the previous sections, relying solely on a GA yields good global exploration but slow and imprecise final convergence. Conversely, using only a local deterministic method such as SQP provides surgical precision, but the algorithm is blind and bound to fail or stall if not provided with a near-perfect initial guess.

To address today's astrodynamic challenges, the most powerful and effective strategy consists of hybridising the two paradigms. A hybrid GA-SQP algorithm combines the broad view of stochastic search with the precision of differential calculus, operating in two distinct sequential phases.

In the first phase, the GA evaluates thousands of candidate trajectories. Since the GA cannot solve the differential equations of motion exactly, the quality of a candidate trajectory w is assessed through a penalised Fitness Function $F(w)$. In addition to rewarding low propellant consumption $J(w)$, the system applies heavy penalties P_k when constraints are violated.

The objective of this phase is not to find a mission-ready trajectory, but a topologically sound one: the GA must sift through the gravitational chaos and deposit its best individual exactly within the attraction basin of the true global minimum. Once the explorer has found the correct valley, its task is complete.

At this point, the best trajectory found by the GA, $w_{GA,best}$, which is geometrically correct but physically rough and does not meet mission tolerances, is directly injected as the deterministic initial guess for the SQP algorithm:

$$\mathbf{X}_{SQP,0} \equiv \mathbf{w}_{GA,best} \tag{4.9}$$

The SQP takes over the solution and activates its network of gradients and parabolic approximations.

The SQP algorithm is then free to express its full potential: it converges rapidly in a matter of seconds, distributes the ΔV exactly, eliminates integration defects, and reduces the high-fidelity model error down to tolerances on the order of 10^{-8}.

From a mathematical standpoint, the integration of the local SQP solver transforms the GA's search space, artificially expanding the attraction basins. If the GA lands even only on the edge of a promising valley, the SQP instantly slides it to the exact bottom. This means the GA does not need to precisely identify the perfect coordinates, it only needs to get close enough to the target.

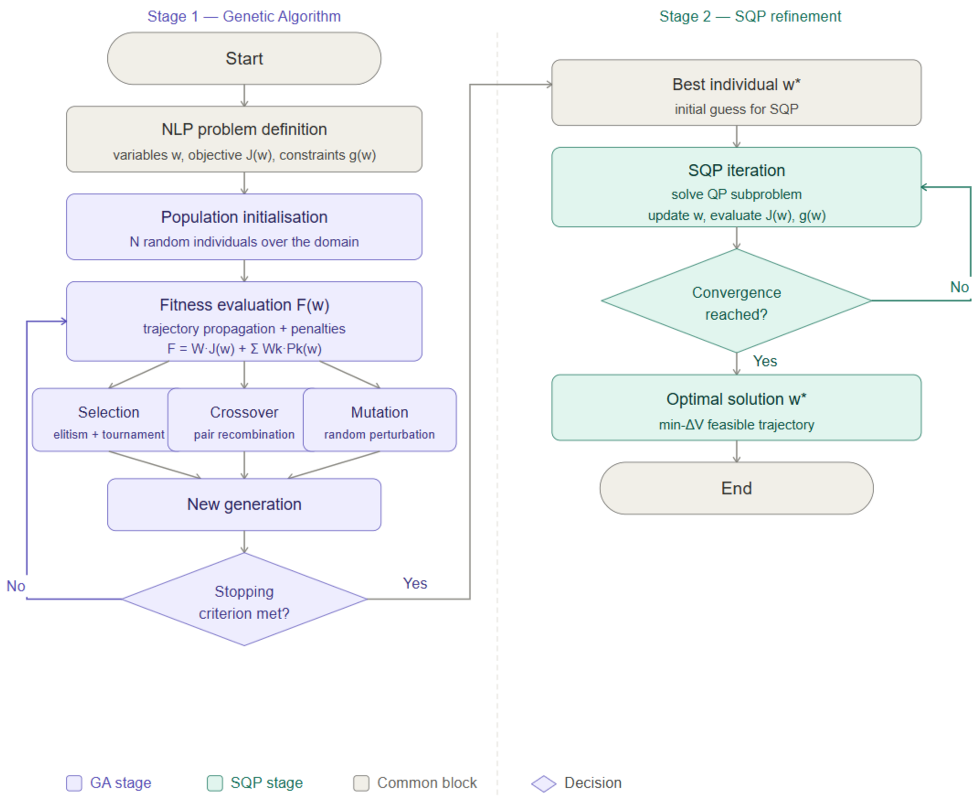

Figure 4.3: GA+SQP flowchart

The result of this hybridisation is a robust and fully automated astrodynamic engine. It eliminates the frustrations associated with manual synthesis of initial guesses that are bound to fail, and enables the autonomous design of high-precision transfers to the Lunar Gateway [28, 26].

Chapter 5

Methodology

Using MATLAB software, a solver was implemented to perform orbital transfer optimizations. The logical process consists of several phases: a problem pre-processing phase in which the best initial data, useful to guide the optimization, are analyzed and determined through the theoretical knowledge of the astrodynamics problem and the computational capability of the adopted tool; the genetic optimization phase, which is the most computationally expensive, at the end of which a rapid post-processing of the results is performed to determine whether the solution is physically valid; the SQP refinement optimization phase leads to the final result by improving the previous solution; the process ends with a detailed analysis of the results, comparison with theoretical expectations, and verification of the physical validity of the solution.

5.1 SPICE Toolkit

The SPICE toolkit, developed by NASA's Jet Propulsion Laboratory, represents one of the reference tools for the geometric and dynamic analysis of space missions. The SPICE environment provides a set of libraries and databases dedicated to the accurate description of the position, orientation, and kinematics of celestial bodies, spacecraft, and reference frames, allowing orbital mechanics problems to be treated with high physical and temporal consistency.

In this context, the toolkit is used to obtain the dynamic states of the bodies involved in the mission, namely position, velocity, and orientation in space as a function of time, within properly defined reference frames. The information is stored in kernels, files containing ephemeris data, physical constants, reference frame transformations, and time information. The modular approach of the toolkit allows different types of kernels to be combined, ensuring consistency in data management and reducing the risk of numerical inconsistencies.

The operating principle is based on querying the ephemerides through routines that, starting from a given epoch, return the state of the desired body with respect to an observer and in a selected reference frame. In the MATLAB environment, this process is carried out through the MICE interface, which allows SPICE functions to be directly called within the numerical environment used for simulations and optimization procedures.

In trajectory design applications, SPICE plays a fundamental role in the accurate definition of the boundary conditions of the dynamical problem. The positions and relative velocities of the Moon, the Sun, and the Gateway station simulation are used to construct transfer arcs, calculate impulsive maneuvers, and evaluate launch windows compatible with mission constraints. The accuracy of the ephemerides is particularly important in interplanetary problems, where even small temporal errors may produce significant variations in orbital parameters and associated propulsive costs. From a computational point of view, the toolkit does not directly perform trajectory optimization, but provides the geometric and temporal support required by the numerical algorithms implemented in MATLAB.

The integration between MATLAB and SPICE is particularly effective in advanced astrodynamics applications, since it combines the robustness of NASA libraries for space data processing with the flexibility of the numerical and optimization tools available in the MATLAB environment. This combination makes it possible to address complex mission analysis problems while maintaining a high level of reliability in the dynamic modeling of the system.

5.2 Conventions

The entire optimization process and all analyses are formulated in a geocentric inertial reference frame (J2000/ECI), ensuring that the dynamical model is free from effects due to Earth rotation and that defect constraints are evaluated consistently. A Moon-centered inertial representation is employed during the analysis of NRHO phases, Moon-relative distances, or for the visualization and verification of the results, particularly during departure from the NRHO and transfer toward LLO. Local reference frames may be introduced for the qualitative representation of maneuver geometry, but they are not used either in the propagation or in the optimization process.

Time management is uniform throughout all functions: internal calculations are performed using the ET/TDB time scale, defined as the number of seconds elapsed since January 1, 2000. For a more immediate interpretation of the results, time is subsequently converted, for example by setting the beginning of the transfer as time zero and using days as the unit of measurement; any conversions are applied during the post-processing phase.

Units are standardized in kilometers for position, kilometers per second for velocity, and seconds for time; angles are computed in radians but expressed in degrees for easier visualization. Gravitational parameters, planetary radii, and other derived quantities are used consistently with the units defined above.

5.3 Input settings and Propagation

For the computational purposes of the optimization, it was necessary to construct a decision vector to be provided as input to the MATLAB functions. This vector contains the temporal instants associated with the impulses and the three components of each velocity variation, and it is structured as follows:

$$\mathbf{X} = [t_1, \Delta t_2, \cdots, \Delta t_N, \Delta V_1, \cdots, \Delta V_{N-1}] \tag{5.1}$$

Where t_0 is the time at which the maneuver begins, the i-th Δt is the time elapsed since the previous impulse, and the ΔV terms are vectors containing the three velocity variation components applied at the corresponding instant. The vector has a total dimension of $1 \times (N + 3(N - 1))$, where N is the total maneuver's number of impulses and includes departure, intermediate maneuvers, and arrival. The temporal instants defined in this way, during random generation, avoid the risk of obtaining successive temporal instants smaller than the previous ones, since the i-th time is obtained as the sum of the previous components of vector X. By convention, the initial time is defined with respect to a reference time t_{ref}. The last ΔV is imposed in order to obtain a circular orbit, if the inclination is not fixed, the orbit is made circular while preserving the direction of the velocity at the arrival point: The state vector is computed from the arrival orbital elements and from those corresponding to the circular orbit. The ΔV is the computed as the velocity difference. In the case of fixed inclination, one starts from this circularized orbit and compares its inclination with the target one. An iterative loop is then introduced in which the flight path angle is increased (or decreased) proportionally to the inclination error. The velocity vector of the circular orbit is rotated by this angle along a plane tangent to the sphere whose radius is given by the position vector (thus ensuring that the newly rotated velocity also propagates as a circular orbit). The new inclination is computed and the loop is repeated until the desired inclination tolerance is reached.

$$
\begin{aligned}
& i_0 = inc(\mathbf{r}, \mathbf{v}_0) \\
& \Delta i_k = i_{target} - i_k \\
& \text{while } |\Delta i_k| > \epsilon_i \\
& \Delta\psi_{k+1} = \Delta\psi_k + K\,\Delta i_k \\
& \mathbf{v}_{k+1} = R_k(\Delta\psi_{k+1})\,\mathbf{v}_k \\
& i_{k+1} = inc(\mathbf{r}, \mathbf{v}_{k+1}) \\
& \Delta i_{k+1} = i_{target} - i_{k+1} \\
& \text{end}
\end{aligned}
\tag{5.2}
$$

Where R_k is the rotation matrix, inc is the function used to compute the inclination, and ψ is the flight path angle. Before applying this procedure, it is verified whether the target inclination is actually achievable at the arrival point of the trajectory. By defining δ as the latitude and u as the argument of latitude (properties of the satellite position along its orbit), the following relation holds:

$$
\begin{aligned}
& \sin(\delta) = \sin(u)\sin(i) \\
& u \in [0{,}2\pi] \rightarrow \sin(u) \in [-1{,}1] \rightarrow \\
& \sin(i) = |\sin(\delta)| \rightarrow i \in [|\delta|, \pi - |\delta|]
\end{aligned}
\tag{5.3}
$$

If the inclination does not belong to that latitude-dependent interval, the closest reachable inclination is used inside the loop. It will then be the optimizer's task to adjust the arrival point in order to achieve the desired inclination values [15]. The resulting ΔV is obtained, as in the previous case, by taking the difference between the velocities at arrival and on the rotated orbit.

For both optimizations it is necessary to define the upper and lower bounds of vector X as follows:

$$
\begin{cases}
l = [0, \epsilon, \cdots, -\Delta V_{max}, \cdots] \\
u = [T_{moon}, t_{max}, \cdots, \Delta V_{max}, \cdots]
\end{cases}
\tag{5.4}
$$

Where ϵ is a very small value, T_{moon} is the Moon period, while V_{max} and t_{max} are the maximum magnitude of the velocity variation and the maximum time of flight.

Trajectory propagation is performed compactly within a single function that takes vector X as input. The code computes the number of impulses directly from the vector dimension and then separates it into a variable containing only the times and another containing the ΔV components. It then computes the initial position on the NRHO using the first component of the temporal vector. From this point, a loop repeated $N-1$ times is entered, where the ΔV is added to the current velocity, the trajectory is integrated for the current Δt, and all variables required for the next iteration are prepared.

5.4 Fitness function and non-linear constraints

The fitness function is the function that the optimizer must minimize, and it is constructed differently for the GA and the SQP. In both cases, the sum of the norms of the ΔV terms is considered, representing the total transfer cost, namely the primary objective of the optimization. A fitness function defined only in this way has no capability to guide the algorithm toward the desired final orbit. For the GA, penalties were introduced in order to leave more freedom for the algorithm exploration. The function is therefore defined as the sum of multiple contributions:

$$F(X) = \sum_{i=0}^{N-1} \|\Delta V_i\| + \omega_a \cdot h + \omega_i \cdot i + P_{coll} + P_{apo} \tag{5.5}$$

Where h and i represent the altitude and inclination of the target orbit scaled by a suitable value ω. P_{coll} and P_{apo} are large constant penalties introduced in case of a collision or if the desired minimum apoapsis is not reached (when present).

For the SQP, instead, the fitness retains only the maneuver cost, while target maintenance is ensured by introducing a non-linear inequality constraint function.

$$\mathbf{c}(\mathbf{X}) = \begin{bmatrix} \Delta h - \epsilon_h \\ \Delta i - \epsilon_i \\ h_{apo,min} - h_{apoastron} \\ c_{coll} \end{bmatrix} \leq 0 \tag{5.6}$$

Where c_{coll} assumes a negative value if no collisions occur, while Δh and Δi are the errors with respect to the target orbit (LEO or LLO) compared with the tolerated errors.

Chapter 6

Results

In this chapter, the results obtained from the trajectory optimizations using the methodologies discussed in the previous chapter will be presented. The transfers will use the Lunar Gateway NRHO as the departure orbit and will target both Earth and Moon destinations with different transfer approaches. The arrival orbit will be a circular orbit with fixed altitude and either free or constrained inclination.

6.1 Maneuvers towards Low Earth Orbit

The NRHO is considered the reference orbit for the Lunar Gateway, the lunar space station of the Artemis program. The transfer from an infrastructure in LEO to the NRHO requires a significant velocity increase, making payload transportation within this orbital architecture inefficient. Nevertheless, the NRHO offers unique advantages: its position gravitationally balances the Earth and the Moon, maximizing propellant efficiency, and ensures almost continuous communications with Earth, as well as flexible access to any site on the lunar surface. For these reasons, the study of optimized trajectories from LEO to NRHO is central in the planning of future lunar infrastructure.[30]

This section presents the optimal solutions for direct transfers toward low Earth orbit, analyzes the configurations obtained from the optimization model presented above, and compares the different trajectories and propellant consumptions. It is first necessary to focus on the initial conditions.

In the NRHO, velocity varies as a function of the distance from the Moon. As shown in Figure 6.1, the maximum velocity is reached at periapsis, while much lower velocities are reached at apoapsis, making it the ideal point for escape maneuvers from the lunar sphere of influence or possible plane changes. The plot shows the relative velocity in the lunar reference frame.

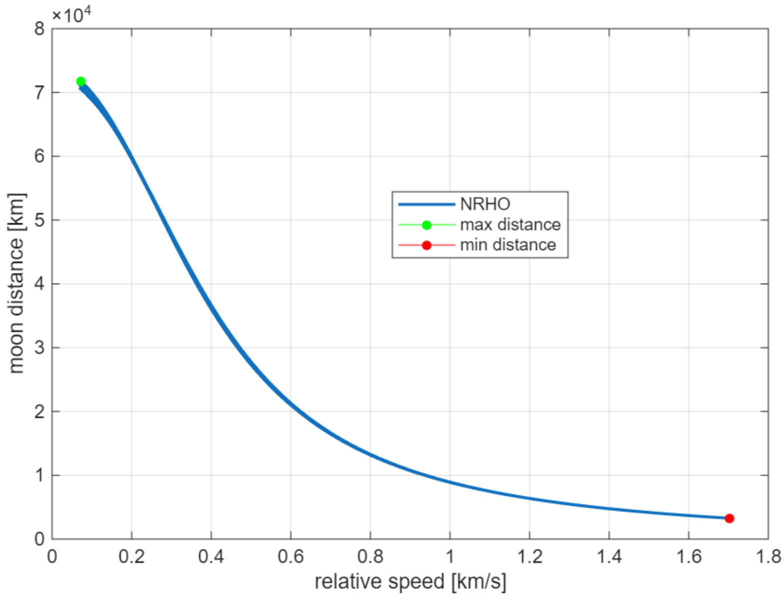

Figure 6.1: Speed as a function of altitude in an NRHO

6.1.1 Single shot direct maneuver

For crewed missions of the Artemis program, NASA selected the In-Direct Transfer as the reference trajectory for human transportation from Earth to the NRHO. The Trans-Lunar Injection inserts the vehicle into the lunar transfer trajectory, which reaches perilune in 4 or 5 days. Although it is less propellant-efficient than low-energy trajectories, it is the operational choice for human transportation on Orion due to its short duration. This type of maneuver represents the architectural reference for all future crewed missions toward the Gateway.[30]

A direct two-impulse trajectory has limited correction capability, and a relatively high consumption is expected. A theoretical ΔV can be estimated by analytically calculating the consumption of a coplanar Hohmann transfer.

$$\begin{aligned}
V_{H1} &= \sqrt{2\mu_e(\frac{1}{r_{moon}} - \frac{1}{r_{moon} + r_{LEO}})} \\
V_{H2} &= \sqrt{2\mu_e(\frac{1}{r_{LEO}} - \frac{1}{r_{moon} + r_{LEO}})} \\
V_{circ} &= \sqrt{\frac{\mu_e}{r}} \\
\Delta V_1 &= V_{circ_{moon}} - V_{H1} \\
\Delta V_2 &= V_{H2} - V_{circ_{LEO}}
\end{aligned} \tag{6.1}$$

These equations do not consider the lunar gravitational influence. If we consider the lunar escape velocity in the lunar reference frame, we obtain:

$$V_{escape} = \sqrt{\frac{2\mu_m}{r}} \tag{6.2}$$

Table 6.1: Results Hohmann maneuver

speed	**value** [km/s]
V_{H1}	0.2
V_{H2}	10.7
$V_{circ_{LEO}}$	7.6
$V_{circ_{moon}}$	1.1
ΔV_1	0.8
ΔV_2	3.1
V_{escape}	0.37

Using the escape velocity value at the apoapsis of the NRHO and a LEO altitude of 500 km, the results reported in Table 6.1 are obtained. We observe that, since the escape velocity is very low and recalling that at the apoapsis of an NRHO the velocity is of the order of 0.1 km/s, the calculated ΔV values can be considered good reference estimates with errors of the order of $10^{-1} km/s$.

The considered transfer is obtained by providing the solver with the optimization variables reported in Table 6.2.

Table 6.2: Input for the optimisation

input	**value**
t0	1/1/2026
h_{LEO}	$500 \pm 5km$
ΔV_{max}	4 km/s
t_{max}	10 days
population size	400
max generations	100

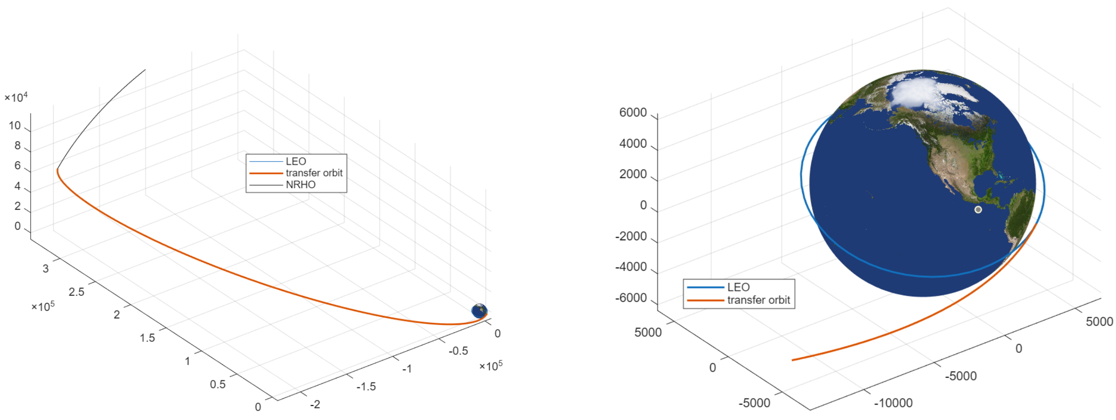

(a) Final trajectory **(b)** Arrival trajectory

Figure 6.2: single shot direct maneuver results

The transfer shown is the result obtained after all optimization processes. The most relevant results are reported in Table 6.3.

	GA optimisation	**SQP optimisation**	unit
inclination	20.0814	20.3647	deg
altitude	503.8918	505.0000	km
ΔV	3.9371	3.9204	km/s
Δt	5.1145	5.0651	day

Table 6.3: Comparison of GA and SQP optimization

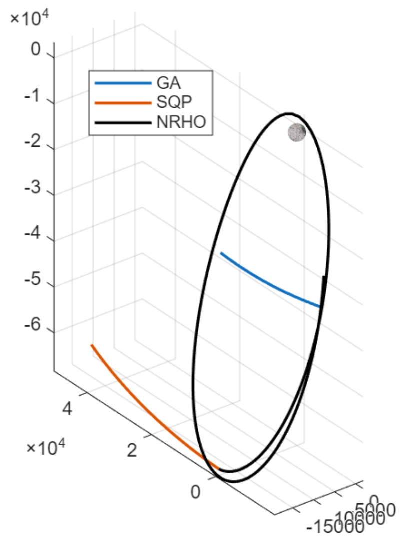

Figure 6.3: Departure trajectories

The effect of the second refinement optimization becomes visible when comparing the two results in the departure maneuver. As visible in Figure 6.3, there is an improvement in the application point of the first impulse, which is moved toward the apoapsis in order to reduce the consumption. This effect is also visible in the bar chart below.

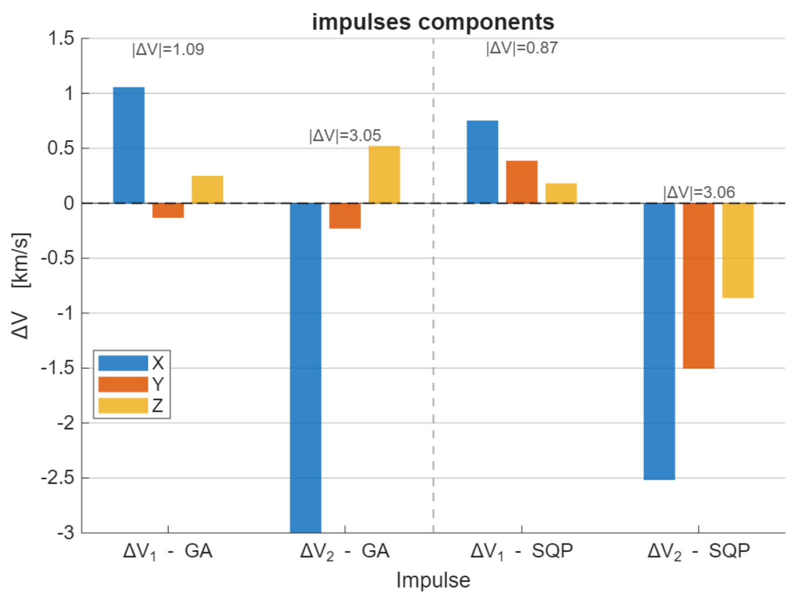

Figure 6.4: components of the starting and arriving pulses

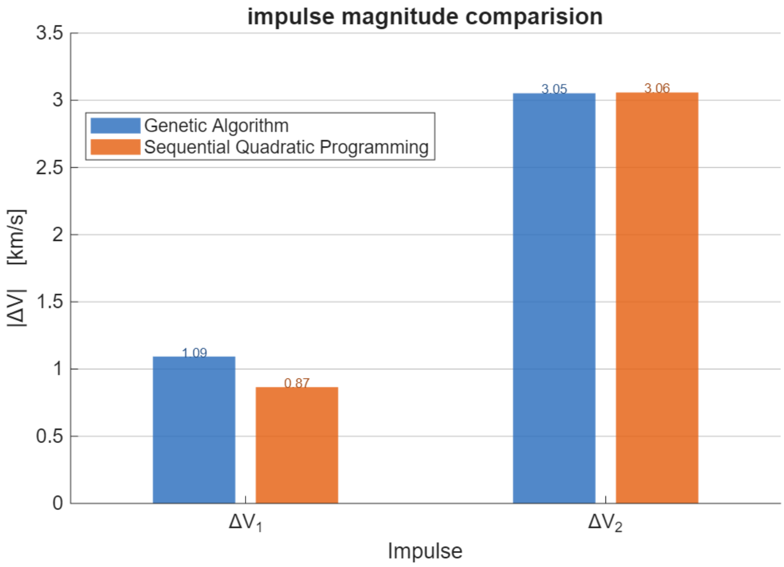

Figure 6.5: norms of the starting and arriving pulses

Keeping the inclination free results in an optimal final inclination that makes the maneuver very similar to a coplanar Hohmann transfer. In the next section, it will be shown that by imposing an inclination different from the optimal one, the consumption for the same type of transfer increases.

6.1.2 Single shot maneuvers with imposed inclinations

Three maneuvers were constructed using the same initial inputs as the previous case, additionally imposing the constraint on the inclination of the reached LEO orbit. In particular, the inclinations were fixed at 20°, 45°, and 90° with an error margin of 0.5°.

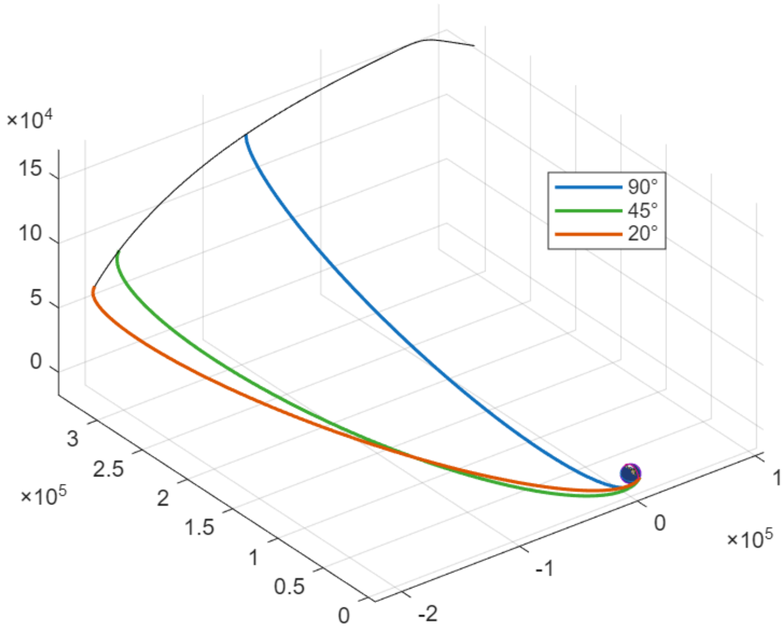

Figure 6.6: single shot maneuvers with imposed inclinations

It is possible to observe that, in this case, the maneuvers with inclinations greater than 20° no longer depart from the optimal NRHO point as in the free-inclination transfer case, since in the new optimum points found, gravitational perturbations produce an almost "free" plane change during the transfer, which ends nearly directly at the target inclination. This effect is shown in Figure 6.7, representing the inclination trend throughout the three transfers. It can be seen that after the first maneuver, the plane change occurs gradually without the use of auxiliary maneuvers.

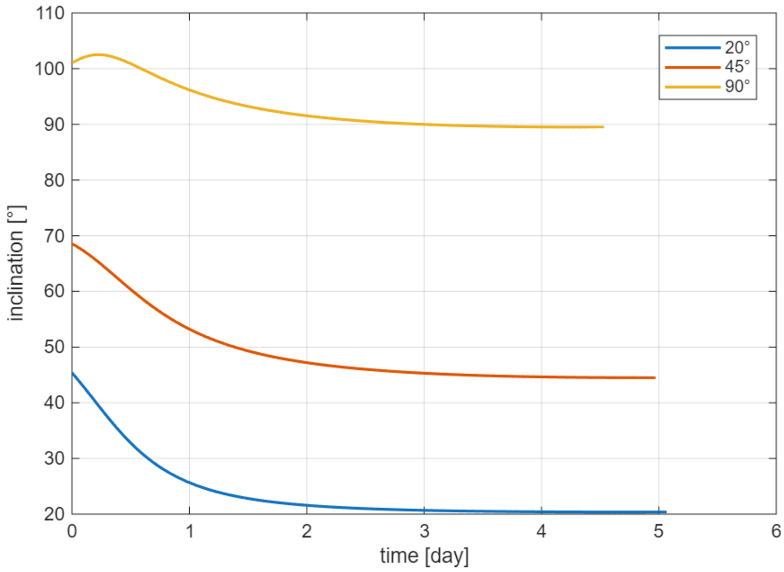

Figure 6.7: inclination trend through trajectories

This beneficial effect, however, is paid for by an additional departure cost for inclinations different from the optimal free-inclination case, while the arrival cost for circularization remains practically unchanged.

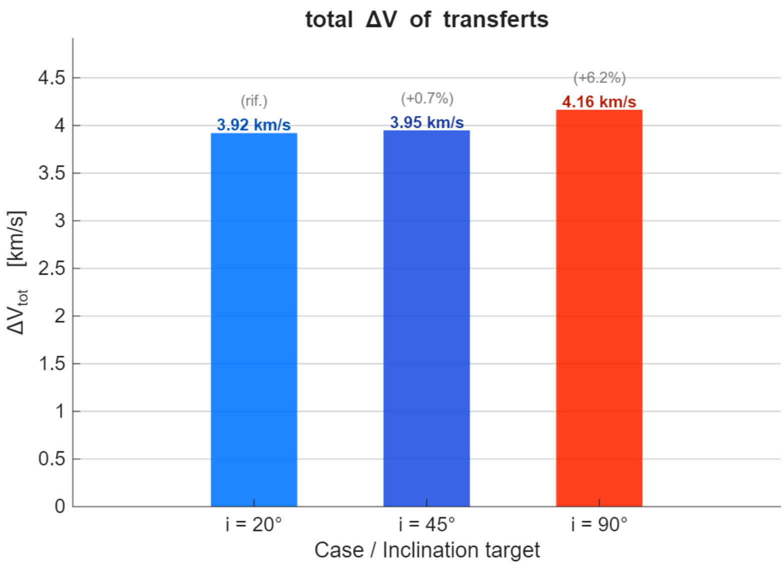

Figure 6.8: pulse bar chart

Finally, it can be observed that the maneuver with the 20° constraint is completely similar to the one without any inclination constraint, as shown in the

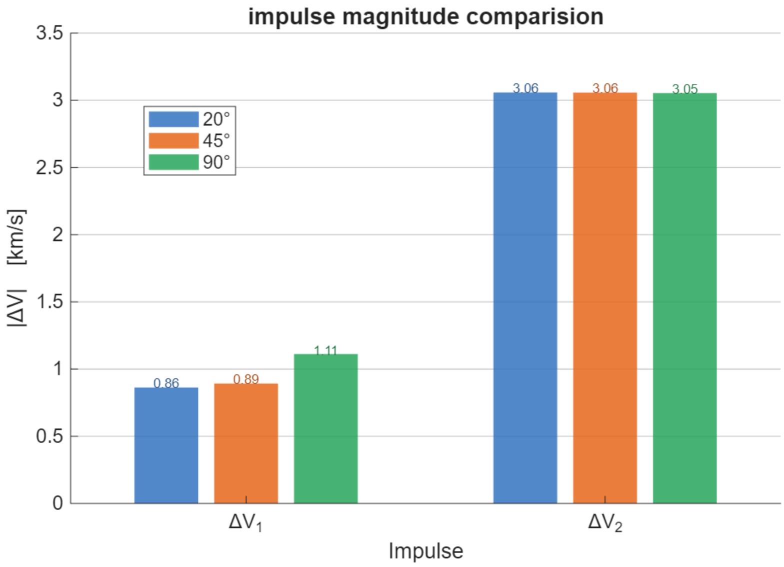

Figure 6.9: comparison of consumption

following table. This demonstrates the effectiveness of the optimization system and the stability of the obtained result.

	free inc	**20°**	**45°**	**90°**	unit
inclination	20.4	20.3	44.5	89.5	deg
altitude	505	505	505	505	km
ΔV	3.92	3.92	3.94	4.2	km/s
Δt	5	4.9	5	4.5	day

Table 6.4: Comparison of 2 impulses maneuvers

The consumption of these transfers could be further reduced by considering the chaotic nature of the Earth-Moon system and increasing the number of impulses in order to better guide the maneuver.

6.1.3 Multiple shot maneuvers

Two relevant cases were analyzed: a transfer with free inclination, in order to test the system response with greater freedom, and a transfer with a fixed inclination of 90°, since, among the previously analyzed cases, it was the most expensive maneuver. The optimization inputs remain the same as in the previous cases, except for the number of impulses, which is increased to 5.

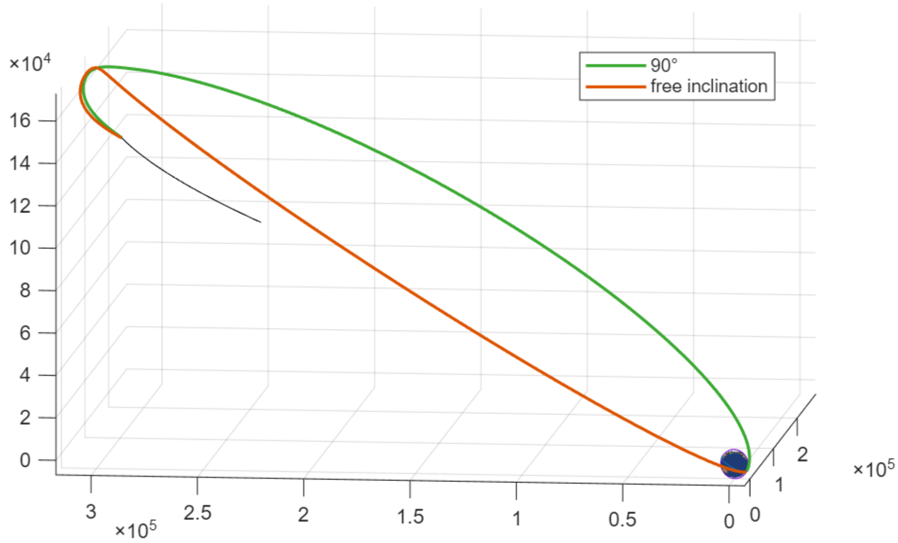

Figure 6.10: multi-shot maneuvers

Unlike the cases discussed in subsection 6.1.2, with the use of multiple impulses the optimizer finds a way to exploit the lunar gravitational field more effectively.

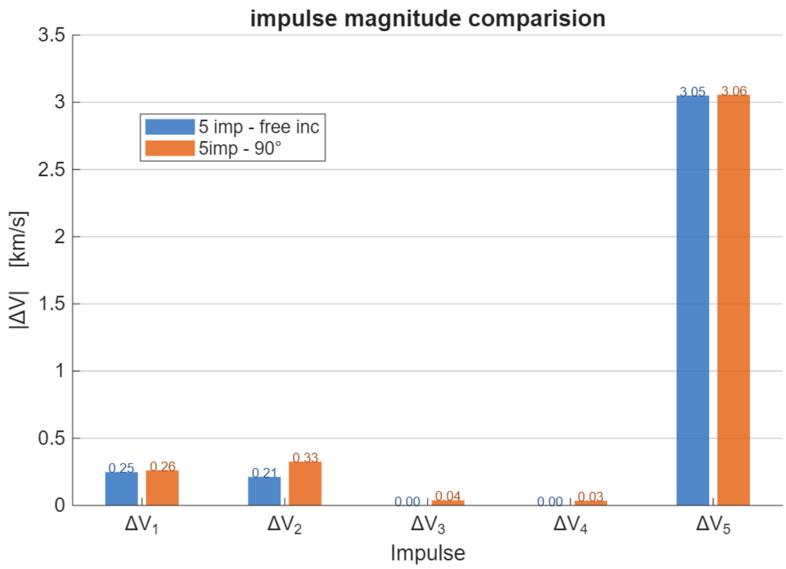

Figure 6.11: pulse bar chart

These plots show that, when more impulses are available, a smaller departure ΔV is required in order to exploit the lunar perturbation more effectively and, with only one additional correction maneuver, enter a low-consumption trajectory toward LEO. In Figure 6.11 it can be observed that, after the final refinement, the impulses actually required to perform this maneuver are only 3. Therefore, a larger number of impulses becomes unnecessary, and inside the optimizer the following impulses converge toward values close to 0 for maneuvers of this type. It can also be observed that the departure impulse reaches a much lower value compared to that of a direct maneuver and, even summing the second impulse, a value of about 0.5 km/s is reached, lower than the 0.8 km/s obtained with the single-shot maneuver.

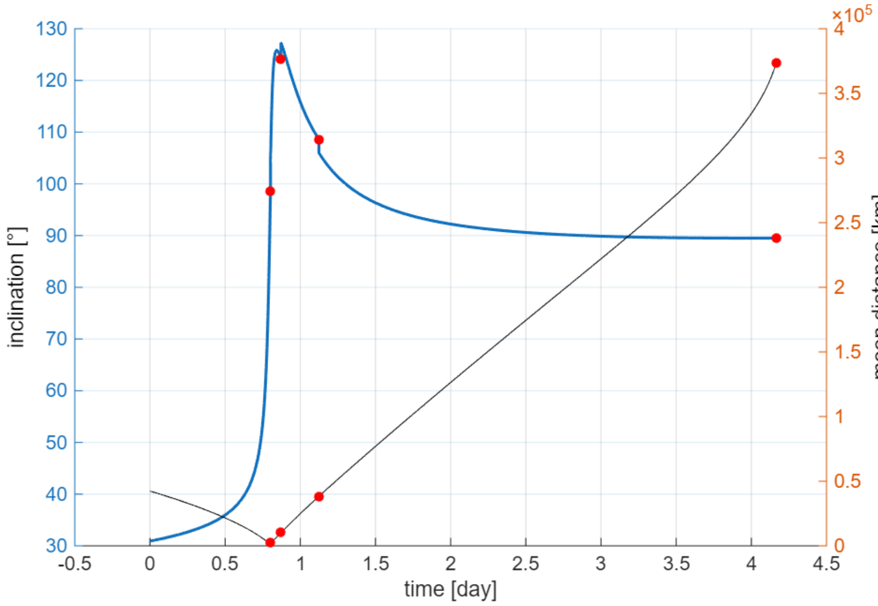

Figure 6.12: inclination trend and moon distance (black) through fixed-inc trajectory

Figure 6.12 shows that significant plane changes are achieved at the minimum distance from the Moon without maneuver cost.

It is possible to compare similar transfers by evaluating the ΔV savings of multi-shot maneuvers. It can be observed that increasing the number of impulses significantly reduces the consumption; however, imposing an inclination constraint still moves the solution away from the ideal minimum consumption.

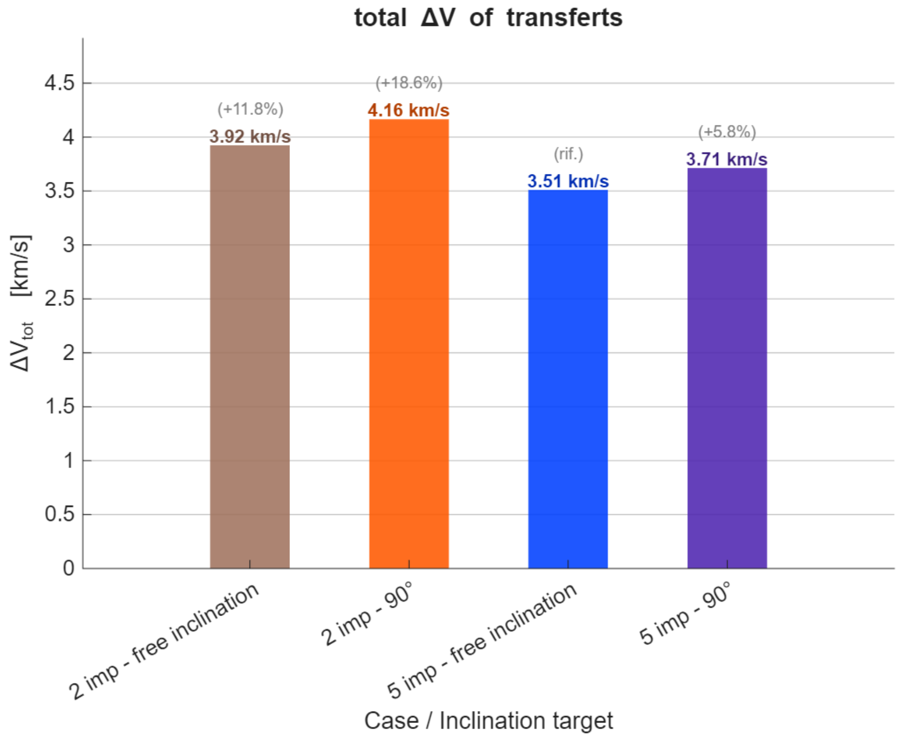

Figure 6.13: comparison of consumption

A different type of maneuver would be required to obtain constant consumption independent of inclination and with even lower costs, accepting significantly longer transfer times.

6.2 Maneuvers towards Low Lunar Orbit

The transfer from LLO to NRHO is a key maneuver in the architecture of crewed lunar missions, since it connects the descent/ascent phase from the surface with the Gateway orbital node. This type of transfer is studied as a fuel optimization problem with multiple impulses, analyzing scenarios with different orientations of the departure and arrival orbits. The optimal transfer strongly depends on the departure epoch; trajectories with longer flight times generally require less ΔV compared to short-duration optimal solutions. The flexibility of this orbital connection is therefore essential to guarantee global access to the lunar surface at any period of the year.[31]

This section discusses transfers toward low lunar orbit. In order to better understand these types of trajectories, Figure 6.1, which shows the velocity trend as a function of altitude for the NRHO, should be recalled.

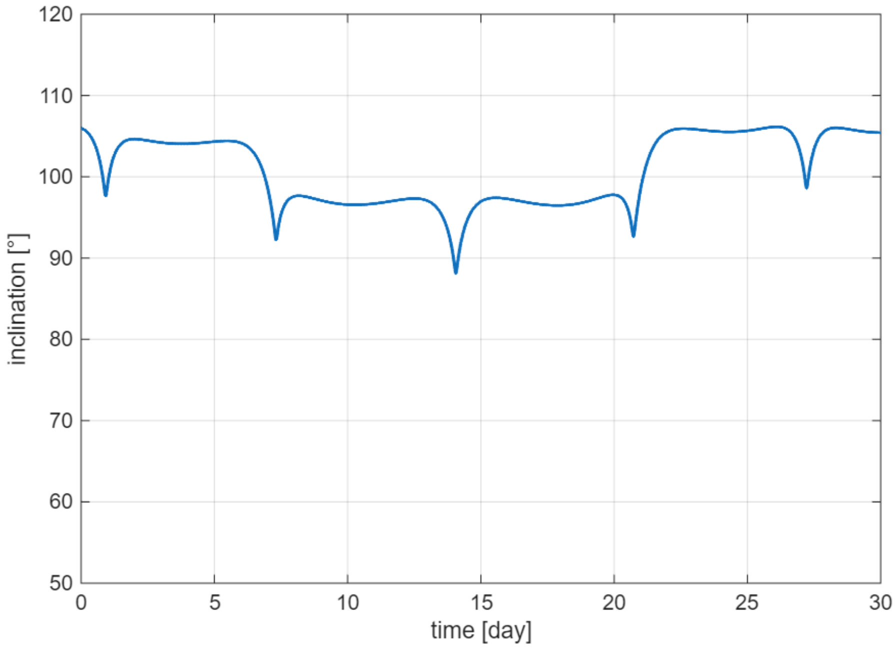

Figure 6.14: inclination trend in NRHO

In this case, it is useful to visualize the inclination trend of the orbit itself in order to understand why, in the free-inclination case, certain inclinations are reached. Figure 6.14 shows that the orbit oscillates around polar inclinations.

6.2.1 Single shot direct maneuver

Within the Artemis program, the direct maneuver from LLO to NRHO is planned for the return of the Human Landing System (HLS) to orbit after descent on the lunar surface. In the planned architecture, the HLS transfer element performs a propulsive maneuver to leave the NRHO and then inserts into a circular LLO at an altitude of 100 km. After ascent from the surface, the vehicle inserts into the perilune of an elliptical transfer orbit and reaches the LLO through a circularization maneuver, remaining in orbit while waiting for the correct orbital alignment before departing again toward the NRHO. This architecture makes the LLO–NRHO transfer one of the most critical maneuvers for astronaut safety in Artemis missions.[32]

With only 2 impulses and free inclination, the transfer is expected to depart from a point of the NRHO lying approximately on the same orbital plane as the target LLO. In order to estimate a reference consumption, the ΔV of two Hohmann-type transfers is compared, one departing from periapsis and one from apoapsis, using equations (6.1).

Table 6.5: Results Hohmann maneuver

speed [km/s]	NRHO apo	NRHO peri
V_{H1}	0.059	1.1
V_{H2}	2.3	1.8
$V_{circ_{LLO}}$	1.6	1.6
V_{NRHO}	0.06	1.7
ΔV_1	1e-3	0.6
ΔV_2	0.63	0.2
ΔV_{tot}	0.63	0.8

Table 6.5 shows that departure from apoapsis is more convenient, mainly thanks to the very small first impulse that still allows the low orbit to be reached.

The resulting transfer is obtained by providing the solver with the optimization variables reported in Table 6.6.

Table 6.6: Input for the optimisation

input	value
t0	1/1/2026
h_{LLO}	$100 \pm 5km$
ΔV_{max}	1.2 km/s
t_{max}	3 days
population size	400
max generations	100

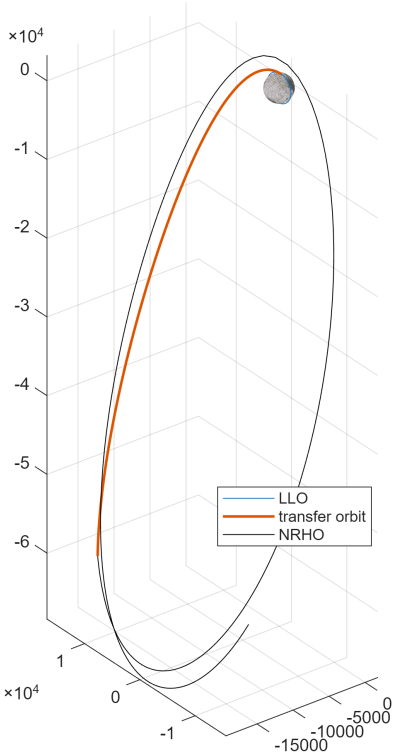

(a) SQP

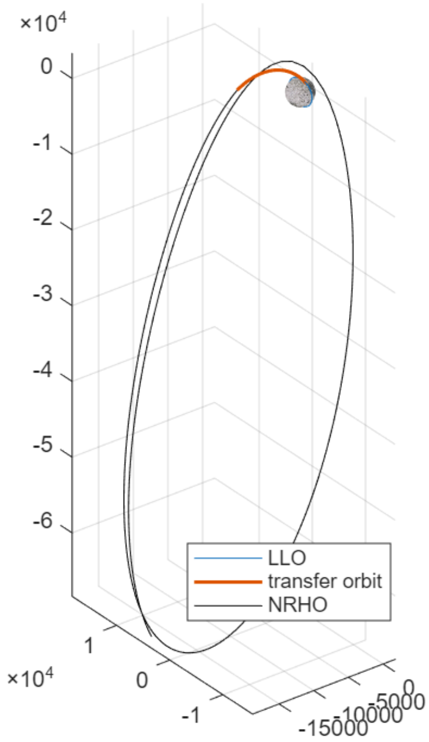

(b) GA

Figure 6.15: single shot trajectory in LLO

As expected from the initial estimates, the transfer begins at a point very close to apoapsis. The results reported in Table 6.7 show, consistently with the estimates, that the maneuver performed at periapsis has a higher consumption, although with a much shorter duration. Since the optimizer has no time constraints, it converges toward the lowest-consumption solution.

	GA optimisation	**SQP optimisation**	unit
inclination	88.0689	92.5991	deg
altitude	105.0000	105.0000	km
ΔV	0.7754	0.6339	km/s
Δt	0.1222	1.9997	day

Table 6.7: Comparison of GA and SQP optimization

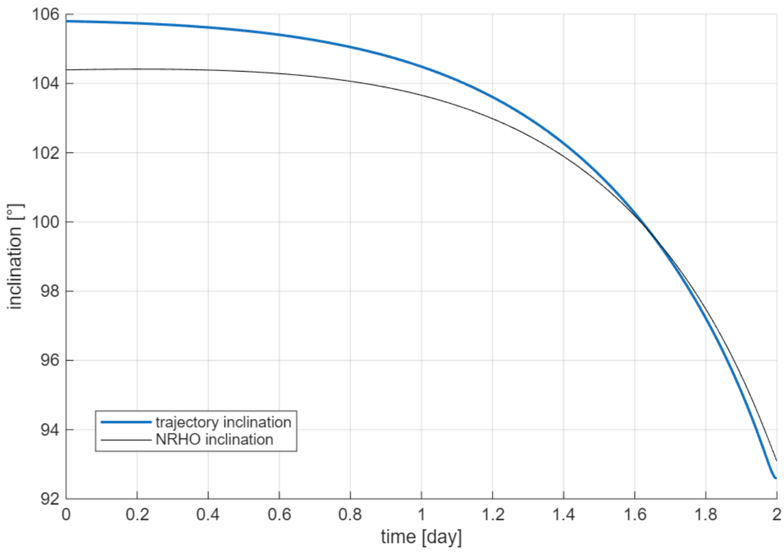

Figure 6.16: transfer inclination trend

A noteworthy result is reported in the plot above, showing that throughout the entire maneuver duration, the inclination remains very close to that of the NRHO, almost completely eliminating plane-change costs.

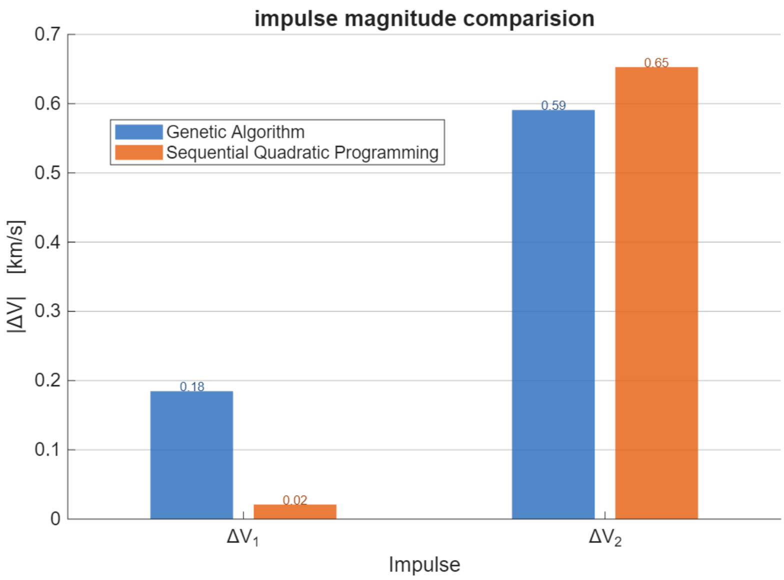

Figure 6.17: bar chart norms

Comparing the ΔV values before and after the refinement, it can be observed that there is a significant reduction in the departure impulse, although with a slight increase in the arrival impulse. This is caused by the fact that a quasi-elliptical maneuver departing from the apoapsis of the NRHO arrives with a velocity much lower than that required to circularize the orbit. In the GA case, instead, the departure point occurs at a lower altitude, therefore the difference with the arrival velocity is smaller.

6.2.2 Multiple shot maneuver with high apoapsis

For uncrewed missions in which flight time is not a stringent constraint, bi-elliptical or low-energy trajectories are used, exploiting the gravitational perturbations of the Sun and Earth to reduce the total ΔV. An example of this approach is the Extended Perilune Rendezvous Method (EPRM), which reduces the required consumption by placing the spacecraft in a lunar ellipse for more than two weeks before inserting into NRHO. This type of trajectory, developed within JAXA studies on the HTV-X for Gateway resupply, is conceptually similar to bi-elliptical trajectories: the vehicle moves significantly away before returning toward the target orbit.[33]

A maneuver of this type allows the consumption to be decoupled from the inclination of the target LLO. It follows the principle of a bi-parabolic transfer with a plane change at apoapsis, theoretically placed at infinity with zero cost. The only cost would be entering the transfer trajectories, which more realistically are elliptical outbound and inbound arcs. For an estimate, the two trajectories can be modeled as Hohmann transfers (6.1) adding a plane change ΔV performed at apoapsis.

$$\Delta V_{\Delta i} = 2V_{tan} \sin(\Delta i) \tag{6.3}$$

Figure 6.18 shows the behavior of the plane-change cost as a function of the apoapsis distance for a 90° inclination change. It can be observed that at distances greater than 2×10^5 km the cost of the plane change becomes negligible, at the expense of a longer transfer time.

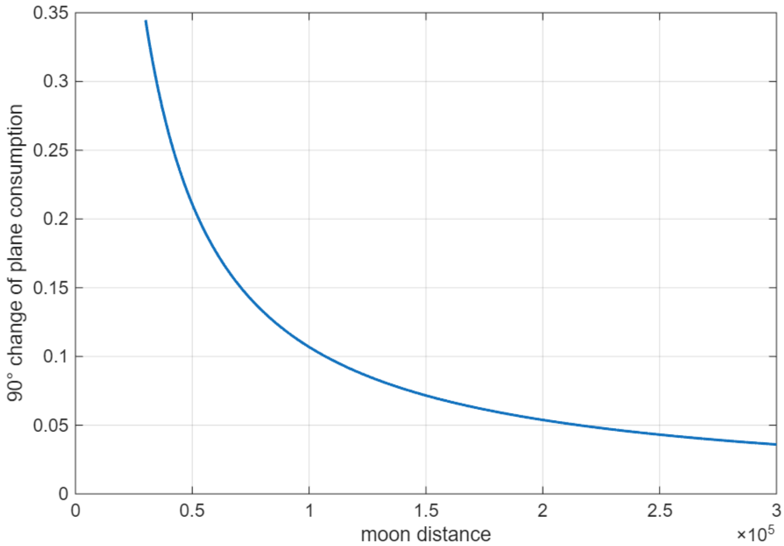

Figure 6.18: ΔV of plane change as a function of Moon distance

Table 6.8: Results bi-elliptical maneuver with 2×10^5 km altitude

speed	**value** [km/s]
ΔV_1	0.1
ΔV_{apo}	0.01
ΔV_2	0.67
$\Delta V_{\Delta i}$	0.05

In practice, such a maneuver is difficult to execute due to the chaotic nature of the Earth–Moon system, but it is useful for comparison with the obtained results. The optimized transfer is obtained using the same input parameters as the previous case, except for the number of impulses, set to 4, and the maximum transfer time, set to 50 days. Additionally, a constraint is introduced on the maximum altitude range, from 2 to 2.5×10^5 km, to guide the optimizer toward this class of trajectories.

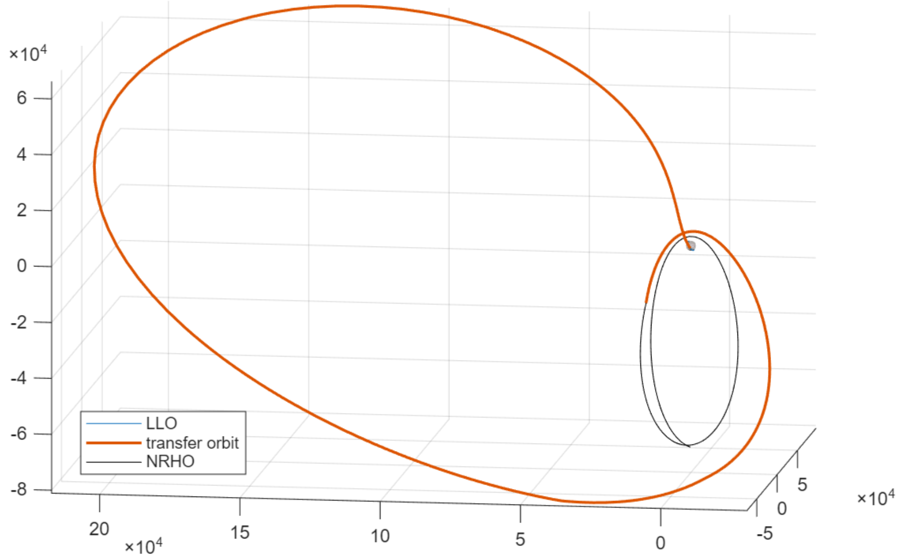

Figure 6.19: Multiple shot maneuver with high apoapsis

In the resulting maneuver, it can be observed in Figure s 6.20 that the first three impulses are mainly trajectory corrections and have little effect on the inclination change, which occurs almost entirely due to gravitational perturbation. It can also be seen that the departure point lies in an intermediate region of the NRHO, with an extremely small impulse that is nonetheless sufficient to place the spacecraft on a trajectory that uses lunar gravity as a slingshot to move away from the Moon.

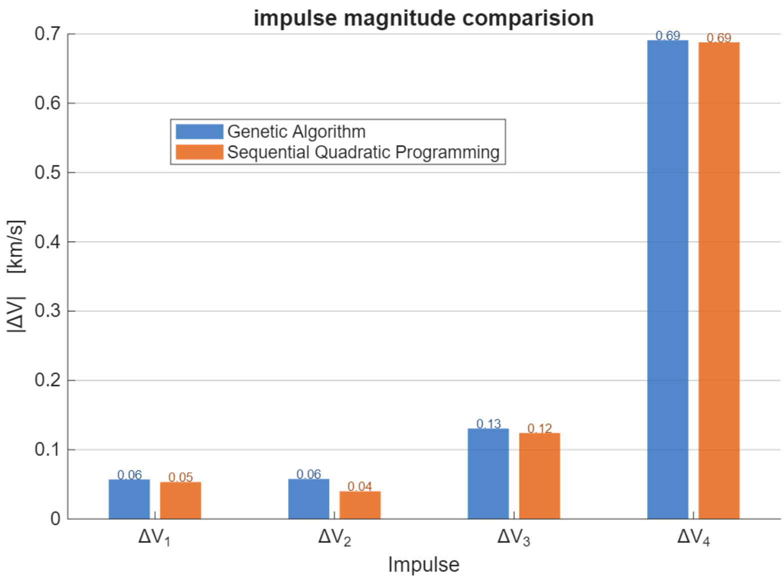

Figure 6.20: impulses bar chart

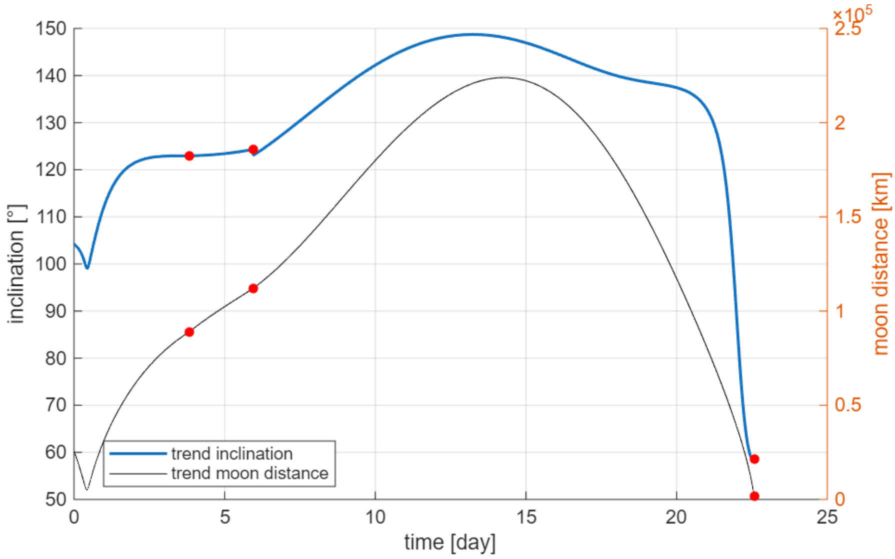

Figure 6.21: inclination trend

It is worth noting that the circularization impulse is similar to that of the 2-impulse maneuver 6.17. Overall, the direct transfer has lower consumption because it does not require intermediate stabilization impulses; however, it is strongly affected by the inclination constraint, as shown in Subsection 6.2.3, making the bi-elliptical-like transfer advantageous for large inclination changes.

	GA optimisation	**SQP optimisation**	unit
inclination	73.8272	58.6380	deg
altitude	105.0000	105.0000	km
ΔV	0.9367	0.9054	km/s
Δt	22.5108	22.5754	day

Table 6.9: Comparison of GA and SQP optimization

6.2.3 Comparison of variable inclinations

Transfers previously discussed were computed by fixing different LLO target inclinations in order to evaluate their effect on fuel consumption. A discrete number of transfers at different inclinations was considered for both the 2-impulse and 4-impulse cases, in order to compare the dependence of ΔV on inclination and to visualize the corresponding trajectory changes. Only three transfers are shown graphically as representative examples to better illustrate the results.

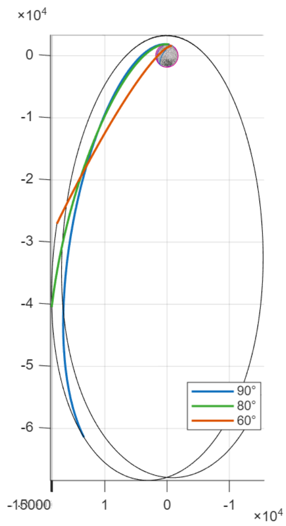

Figure 6.22: single-shot trajectories

It can be observed that, as inclination increases, the transfer departs from a higher point of the NRHO, since, as shown in Figure 6.16, the inclination slightly decreases while approaching the target inclination. In addition, the first impulse changes the trajectory plane significantly and leads to higher consumption because it is less able to exploit perturbations compared to the optimal case. For this reason, the transfer duration decreases as the inclination moves away from the optimal one.

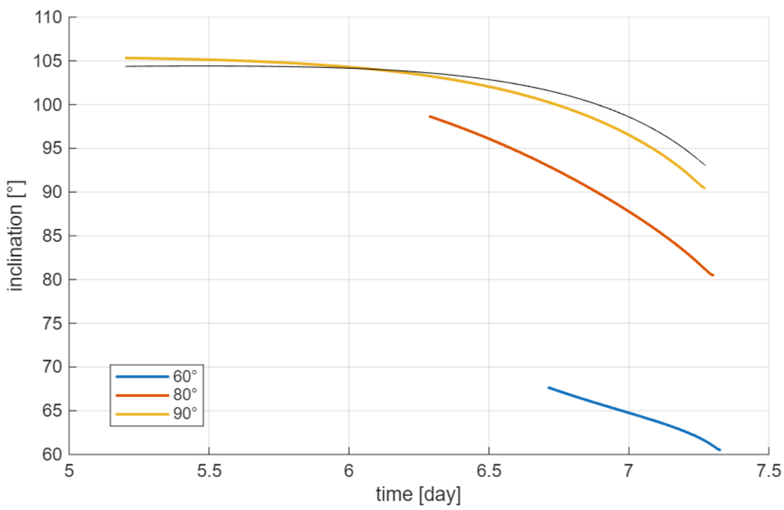

Figure 6.23: inclination trend

In the 4-impulse case, instead, only minor differences are observed both in the transfer geometry and in the inclination profile. The greater maneuvering freedom and the larger distance from the Moon make the difference in consumption almost negligible with respect to the target inclination; small trajectory adjustments are sufficient to guide the spacecraft into an optimal corridor for any inclination without significant variations in ΔV.

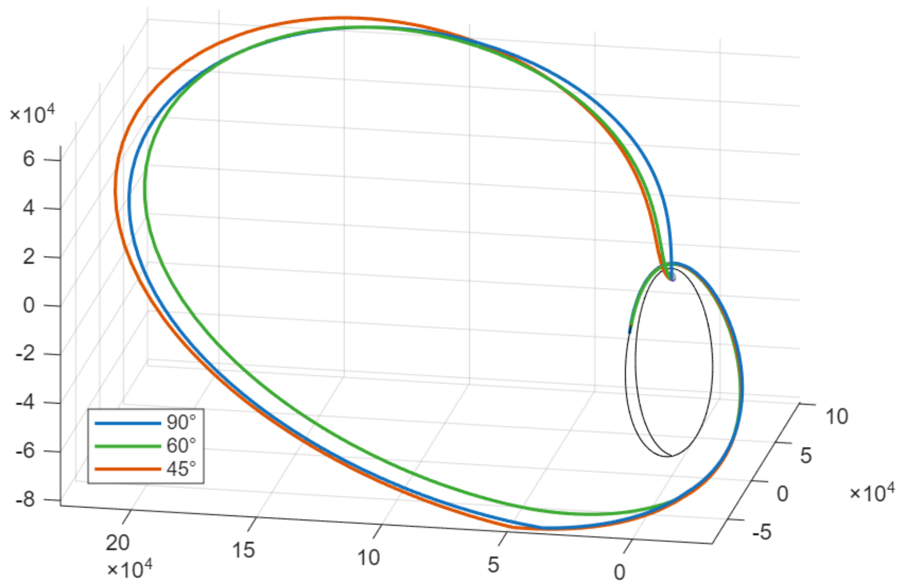

Figure 6.24: multi-shot trajectories

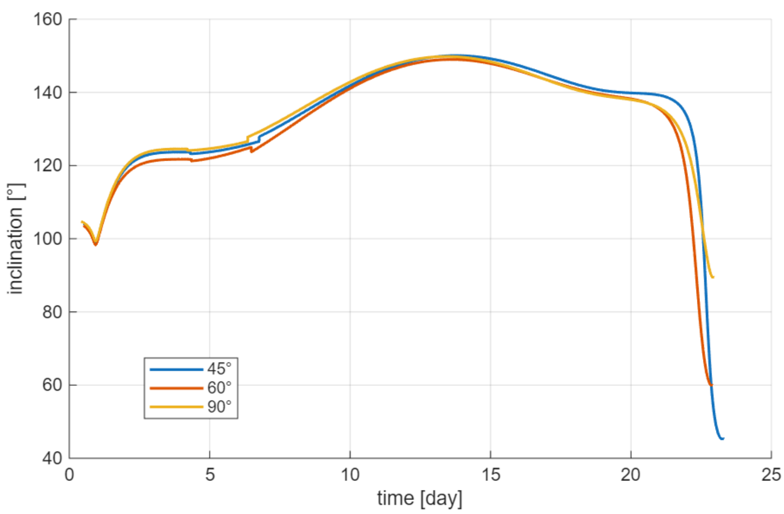

Figure 6.25: inclination trend

To better visualize the results, it is useful to examine how the consumption is distributed in the two types of transfers. It can be observed that the departure ΔV is fairly similar and nearly constant with inclination, although the single-shot maneuver is slightly more efficient due to the closer proximity to the Moon, which makes the arrival velocity closer to that of the LLO. The departure phase shows the most relevant differences: the multi-shot case presents a low and nearly constant consumption, representing the optimal condition for a low-cost escape from the lunar sphere of influence, while the single-shot case shows a parabolic trend with a minimum at the free-inclination configuration, consistent with previous results.

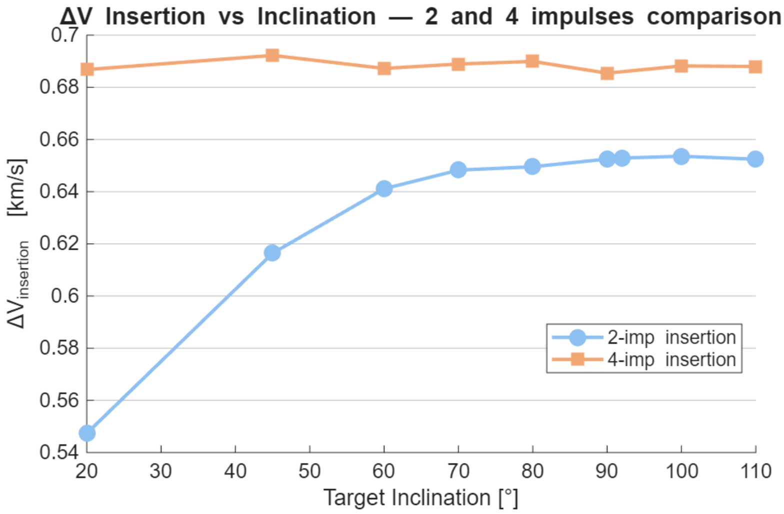

Figure 6.26: Arrival shot

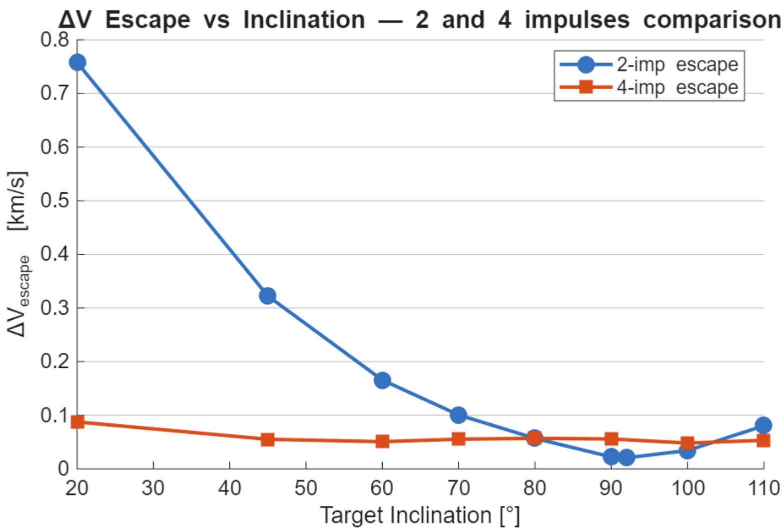

Figure 6.27: Departure shot

More generally, the single-shot transfer is convenient for arrival regions with polar inclinations, while for target inclinations below 45° and for both prograde and retrograde orbits (greater than 135°), it becomes more efficient to first move away from the Moon in order to achieve more effective plane changes, at the expense of longer ToF.

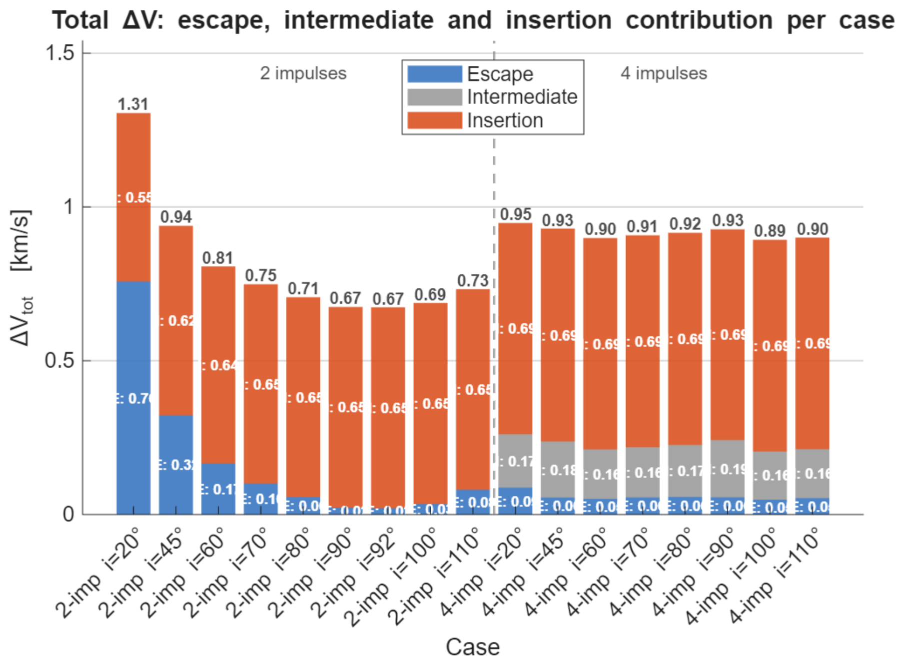

Figure 6.28: full ΔV comparison

6.3 Results and Analysis

The GA–SQP combination is based on the observation that the two algorithms have complementary and almost perfectly opposite characteristics: the GA is robust and global but imprecise; SQP is precise and fast but local and sensitive to initialization. The hybrid approach exploits the convergence of one as the initial condition for the other, resulting in an optimizer that is both globally exploratory and locally accurate.

The operational scheme is structured in two sequential phases: global exploration and local refinement. The GA is run with a sufficient number of generations to identify the attraction basins of the most promising minima. The objective is not to converge to the minimum, but to locate the region of the solution space where the global minimum lies. A stopping criterion based on stagnation of the best fitness or computational budget is typically used. The best individuals of the final GA population are used as initial points for SQP. Each run converges rapidly to the local optimal solution within its attraction basin. The solution with the lowest ΔV is selected as the approximate global optimum. The final solution is validated against mission constraints, and trajectories may be numerically propagated with high fidelity for verification.

The computational advantage of this scheme compared to a pure GA is substantial. The GA spends most of its evaluation budget in the exploration phase, where precision is not required. The SQP, starting from a point already close to the global minimum, converges in a few tens of iterations. The total cost is therefore lower than that of a GA operating at the same final precision.

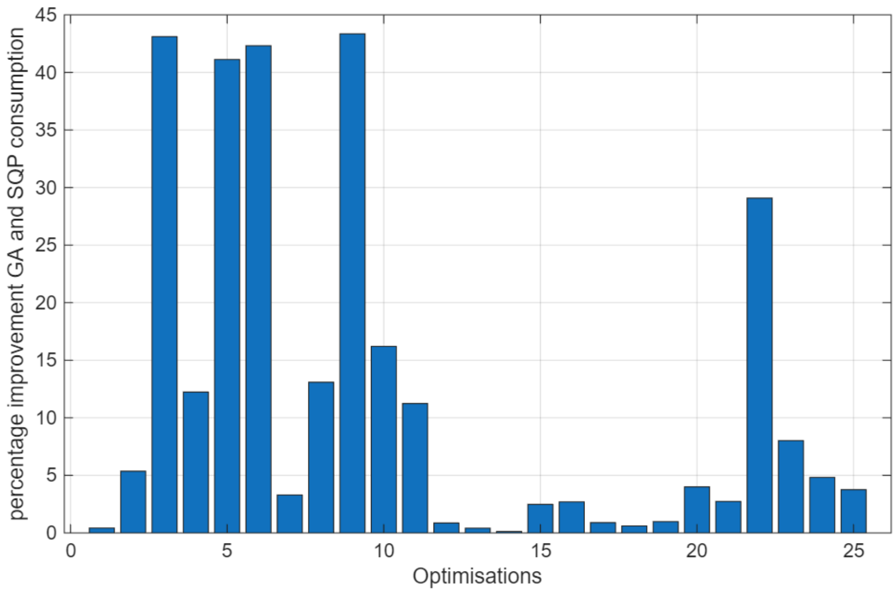

Figure 6.29: ΔV optimisation

The presented data reflect a systematic behavior: the ΔV improvement introduced by the SQP phase is consistent across all considered transfers, with more pronounced gains in cases characterized by more complex optimization landscapes or stochastic behavior of the genetic algorithm.

Chapter 7

Conclusion

This Master's thesis successfully addressed the complex problem of trajectory optimization in the highly nonlinear cislunar environment, proposing and validating a hybrid numerical framework. The primary objective was to compute optimized orbital transfers from the NRHO of the Lunar Gateway towards LEO and LLO, minimizing propellant consumption under varying operational constraints.

From a computational perspective, the results strongly demonstrated the superiority and effectiveness of the hybrid approach GA-SQP over standalone optimization methods. The GA proved highly capable of exploring the chaotic N-body fitness landscape without requiring an accurate initial guess, successfully placing the solution within the correct basin of attraction. Subsequently, the SQP algorithm exploited this topological advantage to rapidly converge to the exact local minimum. This synergy not only guaranteed strict compliance with stringent mission constraints, such as target altitudes and inclinations, but also provided significant advantages in reducing the total ΔV and drastically cutting down the computational times required to reach high-fidelity convergence.

From an astrodynamic standpoint, the application of the solver to specific mission scenarios yielded critical physical insights into cislunar transfer mechanics. Regarding transfers to LEO, the analysis showed that direct, single-shot maneuvers are feasible but energetically expensive, particularly when rigid inclination constraints are imposed. However, introducing multiple impulses allows the spacecraft to better exploit the lunar gravitational perturbation, significantly lowering the departure ΔV and mitigating the penalties associated with severe plane changes. Concerning transfers to LLO, the investigation compared direct insertions with higher-altitude, multi-impulse transfers, such as the Extended Perilune Rendezvous Method or bi-elliptical transfers. It was proven that while direct maneuvers are highly efficient for target orbits closely aligned with the NRHO plane, imposing large inclination changes on short ToF drastically increases consumption. Conversely, multi-shot trajectories with a high apoapsis effectively decouple the plane-change cost from the inclination constraint, allowing the spacecraft to perform nearly free inclination corrections at the apoapsis, at the sole expense of a longer transfer time.

In conclusion, the comparison among the derived trajectories reveals predictable and exploitable patterns that are extremely valuable for mission planners when selecting the optimal transfer architecture under fixed boundary conditions, e.g., final inclination or ToF. The hybrid optimization algorithm developed in this work has proven to be fast, reliable, and versatile. It is well-suited to handle the class of astrodynamic problems examined and establishes a robust foundation for future developments, which could include the integration of low-thrust propulsion systems or the implementation of continuous station-keeping maneuvers within a fully operational NRHO mission framework.

Finally, while NASA has recently paused the Lunar Gateway program in favor of direct surface operations, the astrodynamic relevance of this research remains entirely intact. The optimized maneuvers and the robust GA-SQP solver developed herein are fully transferable to any future spacecraft navigating to an NRHO, confirming the ongoing strategic value of these trajectories for the long-term explorations.

Bibliography

[1] National Aeronautics and Space Administration. *Moon to Mars Architecture - Strategy and Objectives*. URL: https://www.nasa.gov/moon-to-mars-architecture/ (visited on 06/03/2026).

[2] European Space Agency. *ESA - Exploration*. URL: https://www.esa.int/Science_Exploration/Human_and_Robotic_Exploration (visited on 06/03/2026).

[3] I. A. Crawford, M. Anand, C. S. Cockell, H. Falcke, D. A. Green, R. Jaumann, and M. A. Wieczorek. «Back to the Moon: The Scientific Rationale for Resuming Lunar Surface Exploration». In: *Planetary and Space Science* (June 4, 2012). DOI: 10.1016/j.pss.2012.06.002. URL: https://arxiv.org/abs/1206.0749.

[4] National Aeronautics and Space Administration. *Moon to Mars | NASA's Artemis Program*. URL: https://www.nasa.gov/specials/artemis/ (visited on 06/04/2026).

[5] European Space Agency. *Gateway: Lunar Outpost*. URL: https://www.esa.int/Science_Exploration/Human_and_Robotic_Exploration/Exploration/Gateway (visited on 06/04/2026).

[6] M. Caudill, J. Spurbeck, L. De Moudt, A. Zara, B. Tatman, and J. Parker. «A Characterization of the As-Flown Navigation Performance for the CAPSTONE Mission». In: *AAS/AIAA Space Flight Mechanics Meeting*. Paper AAS 25-300. 2025.

[7] National Aeronautics and Space Administration. *What is CAPSTONE?* URL: https://www.nasa.gov/mission_pages/tdm/capstone/index.html (visited on 06/04/2026).

[8] D. Woffinden, R. Eckman, and S. Robinson. «Optimized Trajectory Correction Burn Placement for the NASA Artemis II Mission». In: *AAS/AIAA Space Flight Mechanics Meeting*. Paper AAS 23-062. 2023.

[9] National Aeronautics and Space Administration. *Gateway Space Station*. URL: https://www.nasa.gov/gateway/ (visited on 06/04/2026).

[10] S. Fuller, E. Lehnhardt, C. Zaid, and K. Halloran. «Gateway Program Status and Overview». In: *72nd International Astronautical Congress* (Dubai, AE, Oct. 25–29, 2021). Document ID: 20210022059. Report/Patent Number: IAC-21,A3,2B,13,x6624. International Astronautical Federation, Sept. 27, 2021. URL: `https://ntrs.nasa.gov/citations/20210022059`.

[11] E. M. Zimovan-Spreen, S. T. Scheuerle, B. P. McCarthy, D. C. Davis, and K. C. Howell. «Baseline Orbit Generation for Near Rectilinear Halo Orbits». In: *AAS/AIAA Astrodynamics Specialist Conference*. Paper AAS 23-268. 2023.

[12] The Planetary Society. *'Ignition': A new series of NASA initiatives*. Mar. 25, 2026. URL: `https://www.planetary.org/articles/ignition-new-nasa-initiatives` (visited on 06/15/2026).

[13] H. D. Curtis. *Orbital Mechanics for Engineering Students*. Oxford, UK: Elsevier Butterworth-Heinemann, 2005.

[14] R. R. Bate, D. D. Mueller, and J. E. White. *Fundamentals of Astrodynamics*. Dover Publications, 1971.

[15] M. Battipede. *Meccanica del Volo Spaziale*. Lecture Slides, 01SRMMT. Diapositive del corso. 2023.

[16] L. Mascolo. «Low-Thrust Optimal Escape Trajectories from Lagrangian Points and Quasi-Periodic Orbits in a High-Fidelity Model». Ph.D. Thesis. Politecnico di Torino, 2023.

[17] G. Chen, C. Yang, C. Zhang, and H. Zhang. «Distant retrograde orbits and its bifurcations in Earth-Moon system». In: *Journal of Deep Space Exploration* (2021). Translated title and authors.

[18] R. Zhang. «A review of periodic orbits in the circular restricted three-body problem». In: *Journal of Systems Engineering and Electronics* 33.3 (2022), pp. 611–647. DOI: `10.23919/JSEE.2022.000059`.

[19] E. M. Zimovan, K. C. Howell, and D. C. Davis. «Near Rectilinear Halo Orbits and their Application in Cis-Lunar Space». In: *AAS/AIAA Astrodynamics Specialist Conference*. Paper IAA-AAS-DyCoSS3-125. 2017.

[20] J. Féjoz. «The N-body problem». In: *Université Paris-Dauphine & Observatoire de Paris* (2014). Preprint / Lecture Notes.

[21] E. M. Zimovan. «Characteristics and Design Strategies for Near Rectilinear Halo Orbits Within the Earth-Moon System». MA thesis. West Lafayette, Indiana: Purdue University, Aug. 2017.

[22] D. C. Davis, K. K. Boudad, R. J. Power, K. C. Howell, and D. J. Sweeney. «Heliocentric Escape and Lunar Impact from Near Rectilinear Halo Orbits». In: *AAS/AIAA Space Flight Mechanics Meeting*. Paper AAS 19-867 (Preprint). 2020.

[23] K. Vasiloff, I. Adesina, Z. Wang, K. Mall, and D. A. DeLaurentis. «Trajectory Optimization for Orbit Transfers: Principles, Advances, Case Studies, and Outlook». In: *Aerospace* 12.12 (2025), p. 1087. DOI: `10.3390/aerospace12121087`.

[24] A. Shirazi, J. Ceberio, and J. A. Lozano. «Spacecraft Trajectory Optimization: A review of Models, Objectives, Approaches and Solutions». In: *Progress in Aerospace Sciences* 102 (2018), pp. 76–98. DOI: `10.1016/j.paerosci.2018.07.007`.

[25] N. L. O. Parrish. «Low Thrust Trajectory Optimization in Cislunar and Translunar Space». PhD thesis. University of Colorado at Boulder, 2018.

[26] M. A. Vavrina and K. C. Howell. «Global Low-Thrust Trajectory Optimization through Hybridization of a Genetic Algorithm and a Direct Method». In: *AIAA/AAS Astrodynamics Specialist Conference and Exhibit*. West Lafayette, Indiana, 2008.

[27] F. Cacciatore and C. Toglia. «Optimization of Orbital Trajectories Using Genetic Algorithms». In: *University of Rome 'La Sapienza'*. 2006.

[28] L. Casalino, A. D'Ottavio, G. Fasano, J. D. Pintér, and R. Roberto. «Hybrid Optimization Technique for Finding Efficient Earth–Moon Transfer Trajectories». In: *Algorithms* 19.00080 (2026).

[29] R. I. Woodward and E. J. R. Kelleher. «Towards 'smart lasers': Self-optimisation of an ultrafast pulse source using a genetic algorithm». In: *Scientific Reports* 6.37616 (2016). DOI: `10.1038/srep37616`.

[30] K. Tanaka, H. Ogawa, and K. Yamanaka. «Comparison of transfer trajectory to NRHO and operation plan for logistics resupply mission to gateway». In: *Acta Astronautica* 223 (July 2024), pp. 404–425. DOI: `10.1016/j.actaastro.2024.04.065`. URL: `https://linkinghub.elsevier.com/retrieve/pii/S0094576524004065`.

[31] A. Capannolo and M. Lavagna. «Optimal Impulsive Orbit Transfers from Gateway to Low Lunar Orbit». In: *Aerospace* 11.6 (June 2024), p. 460. DOI: `10.3390/aerospace11060460`. URL: `https://www.mdpi.com/2226-4310/11/6/460`.

[32] R. Whitley, D. Davis, L. Burke, B. McCarthy, R. Power, M. Henderson, and K. Howell. *Enabling Global Lunar Access for Human Landing System Staged at Gateway's NRHO*. 20200002920. National Aeronautics and Space Administration (NASA), 2020. URL: https://ntrs.nasa.gov/citations/20200002920.

[33] S. Takahashi, Y. Saito, and Y. Tsuda. «Rendezvous trajectory design of logistics resupply missions to the lunar Gateway in near-rectilinear halo orbit». In: *CEAS Space Journal* 10 (Mar. 2023). DOI: 10.1016/j.asr.2023.03.001. URL: https://linkinghub.elsevier.com/retrieve/pii/S2468896723000277.